Genetic Complexity in a *Drosophila* Model of Diabetes-Associated Misfolded Human Proinsulin

Soo-Young Park,*.¹ Michael Z. Ludwig,†.¹ Natalia A. Tamarina,* Bin Z. He,†.² Sarah H. Carl,†

Desiree A. Dickerson,† Levi Barse,† Bharath Arun,† Calvin L. Williams,† Cecelia M. Miles,†.³

Louis H. Philipson,* Donald F. Steiner,* Graeme I. Bell,*.‡ and Martin Kreitman†.⁴
*Department of Medicine, †Department of Ecology and Evolution, and †Department of Human Genetics, University of Chicago,

Chicago, Illinois 60637

ABSTRACT Drosophila melanogaster has been widely used as a model of human Mendelian disease, but its value in modeling complex disease has received little attention. Fly models of complex disease would enable high-resolution mapping of disease-modifying loci and the identification of novel targets for therapeutic intervention. Here, we describe a fly model of permanent neonatal diabetes mellitus and explore the complexity of this model. The approach involves the transgenic expression of a misfolded mutant of human preproinsulin, hINS^{C96Y}, which is a cause of permanent neonatal diabetes. When expressed in fly imaginal discs, hINS^{C96Y} causes a reduction of adult structures, including the eye, wing, and notum. Eye imaginal discs exhibit defects in both the structure and the arrangement of ommatidia. In the wing, expression of hINS^{C96Y} leads to ectopic expression of veins and mechano-sensory organs, indicating disruption of wild-type signaling processes regulating cell fates. These readily measurable "disease" phenotypes are sensitive to temperature, gene dose, and sex. Mutant (but not wild-type) proinsulin expression in the eye imaginal disc induces IRE1-mediated XBP1 alternative splicing, a signal for endoplasmic reticulum stress response activation, and produces global change in gene expression. Mutant hINS transgene tester strains, when crossed to stocks from the *Drosophila* Genetic Reference Panel, produce F₁ adults with a continuous range of disease phenotypes and large broad-sense heritability. Surprisingly, the severity of mutant hINS-induced disease in the eye is not correlated with that in the notum in these crosses, nor with eye reduction phenotypes caused by the expression of two dominant eye mutants acting in two different eye development pathways, Drop (Dr) or Lobe (L), when crossed into the same genetic backgrounds. The tissue specificity of genetic variability for mutant hINS-induced disease has, therefore, its own distinct signature. The genetic dominance of disease-specific phenotypic variability in our model of misfolded human proinsulin makes this approach amenable to genome-wide association study in a simple F_1 screen of natural variation.

ODEL organisms are widely employed in mechanistic studies of human Mendelian disease (Bedell *et al.* 1997a,b; Chintapalli *et al.* 2007; Lieschke and Currie 2007; Ocorr *et al.* 2007; Passador-Gurgel *et al.* 2007; Schlegel and Stainier 2007; Lessing and Bonini 2009). They are likewise

Copyright © 2014 by the Genetics Society of America doi: 10.1534/genetics.113.157602

Manuscript received September 18, 2013; accepted for publication October 22, 2013; published Early Online November 26, 2013.

Available freely online through the author-supported open access option.

Supporting information is available online at http://www.genetics.org/lookup/suppl/doi:10.1534/genetics.113.157602/-/DC1.

Microarray data have been submitted to the GEO database (http://www.ncbi.nlm.nih.gov/geo) under accession no. GSE43128.

¹These authors contributed equally to this work.

²Present address: FAS Center for Systems Biology, Harvard University, 52 Oxford St., Cambridge, MA 02138.

³Present address: Augustana College, 2001 S. Summit Ave., Sioux Falls, SD 57197. ⁴Corresponding author: Department of Ecology and Evolution, University of Chicago, 1101 E. 57th St., Chicago, IL 60637-1573. E-mail: martinkreitman@gmail.com. an important resource for investigating the genetic underpinnings of continuously varying quantitative traits (Palsson and Gibson 2004; Telonis-Scott et al. 2005; Wang et al. 2005, 2006: Dworkin and Gibson 2006: Bergland et al. 2008: Gibson and Reed 2008; Ayroles et al. 2009; Dworkin et al. 2009; Goering et al. 2009; Mackay et al. 2009, 2010, 2011). Numerous models of human disease have been established in the fly (reviewed in Pandey and Nichols 2011), including transgenic models of diseases ranging from neurodegeneration/retinal degeneration (Bilen and Bonini 2005; Ryoo et al. 2007; Lessing and Bonini 2009; Yu and Bonini 2011) to cancer (Rudrapatna et al. 2012). Success with genetic screens to identify suppressors and enhancers of disease when mutants are overexpressed in a developing tissue, such as the eye-antennal imaginal disc, suggested to us that it might be possible to generate a fly model of misfolded insulin-associated diabetes.

A number of dominant mutations in human proinsulin have been identified in patients with permanent neonatal diabetes (Stoy et al. 2007, 2010). One class of these involves mutations leading to an unpaired cysteine. The mutation of Cys-96 to Tyr—hINS^{C96Y}—abolishes a disulfide bridge between the A and B chains of the polypeptide, causing proinsulin to misfold and accumulate in the endoplasmic reticulum (ER). Induction of the unfolded protein response (UPR), caused by ER stress, ultimately leads to pancreatic β-cell death (Oyadomari et al. 2002; Hartley et al. 2010). Mutant insulininduced diabetes may also be a model for the more common type 2 (adult onset) form of diabetes, where increased demand for insulin overwhelms the pathways regulating protein folding and trafficking. In this case, the accumulation of misfolded wild-type proinsulin in the ER is hypothesized to trigger pathways that respond to loss of proteostatic control (Oyadomari et al. 2002; Scheuner and Kaufman 2008).

Many signaling mechanisms regulating proteostasis—the dynamics of protein expression and turnover including folding, processing, transport, regulation, and degradation—are conserved between fly and human (Geminard et al. 2009; Karpac and Jasper 2009; Haselton and Fridell 2010; Biteau et al. 2011). Misfolded alleles of rhodopsin, for example, cause age-related retinal degeneration in both species. In the fly model, overexpression of ninaE (a mutant allele of the fly ortholog of human rhodopsin-1) in the eye-antennal imaginal disc induces ER stress-associated UPR and proapoptotic signaling, resulting in adult-onset eye degeneration (Ryoo et al. 2007; Kang and Ryoo 2009; Mendes et al. 2009; Kang et al. 2012). Strongly conserved signaling mechanisms in these pathways led us to reason that overexpression of mutant human preproinsulin (hINSC96Y) in the fly would likewise unleash UPR and cell death, thus recapitulating biological processes acting in the human form of the disease.

To test this prediction we created a transgenic model of permanent neonatal diabetes in the fly by expressing hINS^{C96Y} under regulatory control of the UAS-Gal4 system. We drove hINS expression in larval/pupal imaginal discs, precursors of adult structures, and measured the loss of adult tissue, expected if the mutant activated cell death pathways. We also examined phenotypes in flies expressing wild-type human preproinsulin (hINS^{WT}) as a control. Here we describe phenotypic characteristics of this Mendelian model of disease, including sex-specific differences, dosage, environmental sensitivity, and reorganization of gene expression.

In addition, we examined dominant and partially dominant genetic variation in disease severity by crossing a panel of inbred lines derived from a natural population sample [Drosophila Genetic Reference Panel (DGRP)] (Mackay et al. 2012) to a tester stock carrying both the mutant insulin transgene and an eye imaginal disc-specific Gal4 expression driver on the same chromosome (GMR>>hINS^{C96Y}). With Drosophila having 20–40 times greater density of single-nucleotide polymorphisms (SNPs) than human and being genetically variable for most phenotypic traits, we expected this genetic screen to expose abundant genetic variation

for the severity of disease phenotypes. Measuring the effects of natural modifiers in outcrossed flies avoids inbreeding effects in the isogenic lines and better mimics their heterozygosity in natural populations, especially low-frequency variants. Repeated measurements of genetically identical F_1 flies also reduce nongenetic variance components compared to individual measurements, increasing the power to detect genetic differences (Mackay *et al.* 2009). By examining adult eye reduction in F_1 flies, we quantify disease phenotypes in different genetic backgrounds and describe its distribution of effects in a natural population sample.

We then investigated biological properties of the naturally occurring genetic variation unleashed by our model of proteostatic disease. We first determine the correlation structure of hINSC96Y-induced phenotypes in the adult eye and notum when hINSC96Y is expressed in their respective imaginal discs in a set of DGRP lines. We provide evidence for different alleles or loci modifying the disease in the two tissues, contrary to our expectation that the same alleles would be acting. This result led us to investigate genetic variation acting in eye-specific developmental pathways. We measured eye reduction in the same DGRP lines in crosses to two classical dominant eye mutants, *Drop* (*Dr*) and *Lobe* (*L*), and found that both are also uncorrelated with eye reduction induced by hINSC96Y expression. The presence of tissue- and disease-specific modifiers in our model of a human Mendelian disease affirms the suitability of Drosophila as a model for investigating genetically complex forms of human disease.

Materials and Methods

Drosophila stocks

The *Drosophila* stocks used in this study are described in Table 1.

Crosses

Flies were maintained on standard commercial medium at 25°. Mutant and wild-type hINS phenotypes, including adult and imaginal disc morphology and gene expression, were examined in F1 flies produced by crosses between stocks carrying a hINS transgene (M-1 or WT-24) and a tissue-specific Gal4 driver (GMR-Gal4, ap-Gal4, en-Gal4, or dpp-Gal4). To examine hINS phenotypes in outcrossed genetic backgrounds, we crossed DGRP inbred stocks with a "tester" stock in which a Gal4 driver (GMR-Gal4 or ap-Gal4) was recombined onto a second chromosome carrying a hINS transgene (designated GMR>>hINS or ap>>hINS; Table 1). For each cross, and also crosses between DGRP stocks and L or Dr, 5 healthy virgin females from the tester stock were mated with 5-10 healthy males from each the DGRP stocks. Parents were transferred to fresh culture bottles every 2 days for 8 days. Phenotypes were measured separately in a minimum of 10 individuals for each sex. Eye measurements were made on 3to 5-day-old adults only. This particular trait, however, is stable in adults and has good replicability (Supporting Information, Figure S1). The crosses between the tester stock and

Table 1 Drosophila stocks

Stock	Genotype	Reference or source	Comment
hINS transgene			
WT-24; WT-6	P(UAS-hINS ^{WT}) w1118 background	This study	Wild-type human proinsulin; second chromosome insertion site
M-1; M-101	P(UAS-hINS ^{C96Y}) w1118 background	This study	Mutant human proinsulin; second chromosome insertion site
Gal4 drivers			
GMR-Gal4	w*; P{Gal4-ninaE.GMR}12	1104 (Bloomington Stock Center)	Expresses in eye disc morphogenetic furrow
ap-Gal4	ap-Gal4/CyO	25686 (Bloomington Stock Center)	Expresses in developing mesothorax (notum)
en-Gal4	en-Gal4 ciBe/CyO Act5c-GFP	R. Fehon	Expresses in ventral compartment of wing imaginal disc
dpp-Gal4	dpp ^{blnk} -Gal4, UAS-GFP ^{NLS} /TM6B	R. Fehon	Expresses between dorsal and ventral compartments of wing imaginal disc
[Gal4 driver], [hINS]; Gal-	4 driver, hINS same chromosome		
GMR>>hINS ^{WT} , GMR>>hINS ^{C96Y}	w1118; GMR-Gal4, UAS-hINS ^{WT or C96Y} , UAS-GFP/CyO	This study	GMR-Gal4 driver recombined onto hINS-bearing chromosome (WT-24 or M-1)
ap>>hlNS ^{WT} , ap>>hlNS ^{C96Y}	w1118; ap-Gal4, UAS-hINS ^{WT} or ^{C96} /CyO	This study	ap-Gal4 driver recombined onto hINS-bearing chromosome (WT-24 or M-1)
Other stocks			,
Drop (Dr)	w1118; Dr1/TM3, twist-GFP	R. Fehon	Reduced eye size; acts through Jak/Stat pathway in ventral eye development
Lobe (L)	L(1)	318 (Bloomington Stock Center)	Muscle segment homeobox-1 transcription factor; induces apoptosis in developing eye
Scutoid (Sco)	w1118; CyO dfd- YFP/sna ^{Sco}	R. Fehon	Missing bristles on notum
DGRP	Inbred wild lines	Bloomington Stock Center	"Core 38 " used in these experiments

DGRP stocks were generally carried out in a single block to minimize experimental error.

Transgene construction and P-elementmediated transformation

The Gal4/UAS system (St. Johnston 2002) was used for ectopic gene expression of the wild-type and mutant (C96Y) human preproinsulin. Transgenic human preproinsulin wildtype (hINSWT) and mutant (hINSC96Y) flies were generated by subcloning the human preproinsulin cDNA (Bell et al. 1979) into the Drosophila transformation vector pUAST (https://dgrc.cgb.indiana.edu/product/View?product=1000). Transformation was carried out as described in Spradling et al. (1995). Mapping crosses are described in Ludwig et al. (1993). For the UAS-hINSWT and UAS-hINSC96Y constructs, we generated 8 and 19 independently transformed stocks, respectively, each of which contained a single transposon insertion. For each of two constructs (WT and C96Y) at least one insertion in each of the three major chromosomes of Drosophila melanogaster was generated to control for the influence of position effect on transgene expression.

Immunohistochemistry

Drosophila third instar wandering larvae of either sex were dissected in phosphate-buffered saline (PBS). Isolated discs (approximately five pairs per sample) were placed in a glass tube with 4% paraformaldehyde in PBS and incubated for 30–40 min at room temperature. Discs were then washed three times in PBS, 5 min each, and treated with 1% Triton

X-100 in PBS for 30 min at room temperature. Discs were washed again three times in PBS for 5 min each and treated with 5% normal donkey serum (NDS) in PBS. Staining with a mixture of mouse anti-human C peptide (Millipore, Bedford, MA; 1:200) and rat anti-ELAV (Developmental Studies Hybridoma Bank, University of Iowa, Iowa City, IA; 1:200) was performed in PBS with 1% NDS. Secondary antibodies were from Jackson ImmunoResearch. After staining, imaginal discs were removed with a glass pipette coated with NDS, placed in a drop of SlowFade Gold with DAPI (Invitrogen, Carlsbad, CA) antifade solution, and covered with a glass coverslip. Staining was observed with a Leica SP2 laser scanning confocal microscope with 20× or 63× objectives.

Transcriptional profiling

Total RNA from 12 eye imaginal discs from each stock was isolated from wandering third instar larvae, using the MELT Total Nucleic Acid Isolation System (Ambion, Life technologies). The quality and quantity of each RNA sample were checked using a 2100 BioAnalyzer (Agilent Technologies) and Nanodrop 1000 (Thermo Scientific). Amplification of total RNA and synthesis of cDNA were carried out using the Ovation RNA Amplification System V2 (NuGen Technologies) from 100 ng of total RNA. The amplified cDNA was purified using a Zymo-Spin II Column (Zymo Research Clean and Concentrator-25; Zymo Research). Totals of 3.75 μg of fragmented and labeled single-stranded cDNA targets were generated by the FL-Ovation cDNA Biotin Module V2 (NuGen Technologies) and hybridized to each

Affymetrix-GeneChip *Drosophila* Genome 2.0 Array. Four microarrays were used to estimate transcript levels for the F_1 progenies from five crosses (two males and two females each): control (GMR-Gal4 \times w1118) expressing the Gal4 activator protein only, hINS^{WT} line 6 (GMR-Gal4 \times WT-6), hINS^{WT} line 24 (GMR-Gal4 \times WT-24), hINS^{C96Y} line 101 (GMR-Gal4 \times M-101), and hINS^{C96Y} line 1 (GMR-Gal4 \times M-1). The two lines of each genotype, hINS^{WT} or hINS^{C96Y}, were selected to represent moderate and high expression of the hINS transgene. Microarray data are available at the Gene Expression Omnibus (GEO) (http://www.ncbi.nlm.nih.gov/geo) under accession no. GSE43128.

Analysis of microarray data

Intensity data for each feature on the array were calculated from the images generated by the GenChip Scanner 3000 7G (Affymetrix) and the data files were extracted using GeneChip Operating Software (MicroArray Suite 5.0 software; Affymetrix). We performed background subtraction and normalization of CEL files both in dChip (2010.1) software with its default parameter (fifth percentile of perfect match probes as baseline for background subtraction, invariant set for normalization).

Data analysis 1: We used Partek software (v6.5) initially to identify differentially expressed genes in the comparison between GMR-Gal4 background and each transgenic fly (GMR-Gal4/UAS-hINS^{WT} or INS^{C96Y}, four genotypes). Sexes were analyzed separately. A one-way ANOVA was performed with genotype as a fixed effect. All genes for which the effect of genotype was significant at a false discovery rate (FDR) of 10% were further tested to determine whether mean expression of GMR-Gal4/UAS-hINS^{WT} or GMR-Gal4/UAS-hINS^{C96Y} was significantly different from that of the control (GMR-Gal4).

Data analysis 2: The normalized intensity data were $\log 2$ transformed for subsequent analyses implemented using R-bioconductor (v 2.10.0). To compare the transcriptional responses to the expression of wild-type or mutant hINS, we restricted the analysis to a single pair of the transgenic lines, WT-24 and M-1, matched for high level of hINS expression based on quantitative real-time (qRT) PCR, together with the control (GMR-Gal4), and performed independent ANOVA for each array feature under the model $Y_{ijk} = u + L_i + S_j + e_{ijk}$, where L_i is line (i = 1, 2 or 3), S_j is sex (j = 1 or 2), and e_{ijk} is error (k = 1 or 2). We applied the Benjamini and Hochberg procedure (Benjamini and Hochberg 1995) on the resulting P-values to control the FDR.

Quantitative real-time PCR

Total RNA was isolated from heads of 30 adult flies, using Trizol reagent (Invitrogen, Life Technologies), and from eyeantennal imaginal discs from 12 wandering third instar larvae, using the MELT Total Nucleic Acid Isolation System (Ambion). cDNA synthesis was performed using oligo(dT) primer and the Superscript III First-Strand Synthesis System (Invitrogen). qRT- PCR was carried out using a StepOneReal-Time PCR System (Applied Biosystems Inc., Life Technologies) in triplicate. Genespecific sets of primers (Table S1) and SYBR green PCR master mix (Applied Biosystems Inc.) were used to quantify gene expression. Results were normalized to the expression of *rp49*.

Analysis of XBP1 mRNA splicing

Total RNA was isolated from wandering third instar larvae and cDNA synthesized, as described above. To visualize the alternative splicing of the 23-bp XBP1 intron, a diagnostic marker of UPR induction (Cox and Walter 1996; Mori et al. 2000; Shen et al. 2001; Yoshida et al. 2001), PCR was carried out using the D. melanogaster-specific primers 5'-AACAGCAG-CACAACACCAGA-3' (forward) and 5'-CGCCAAG-CATGTCTTGTAGA-3' (reverse), which amplifies fragments of 239 bp for unspliced XBP1 (U) and 216 bp for spliced XBP1 (S). The PCR conditions were initial denaturation at 94° for 3 min; 35 cycles of denaturation at 94° for 30 sec, annealing at 57° for 30 sec, and extension at 72° for 1 min; and a final extension at 72° for 10 min. PCR products were separated by 10% PAGE and visualized by ethidium bromide staining. PCR products were also digested with PstI to better distinguish the spliced and unspliced forms of XBP1 mRNA.

Eye measurement

Low-magnification images were captured with a Zeiss (Carl Zeiss, Thornwood, NY) AxioCam HRc mounted on a Leica MZ16 fluorescent stereomicroscope. For high-magnification images, eyes were mounted in Halocarbon 700 oil (Sigma, St. Louis) and were captured with a Zeiss AxioCam HRc camera on the Zeiss Axioscope microscope.

Three- to 5-day-old adults of the appropriate genotype from each cross (in some experiments following thorax measurement) were placed on a slide containing a thin layer of silicone vacuum grease (Beckman, Fullerton, CA) and mounted in Halocarbon 700 oil under a coverslip supported by capillary tubes. Eyes were photographed using a Leica DFC420 camera mounted on a Leica M205 FA stereomicroscope. The Leica Application Suite software and ImageJ software (rsb.info.nih.gov/ij/) were used to analyze merged Z-stacks taken on the Leica M205 FA microscope. Only eyes with borders and head capsules in the same optical section were analyzed. At least 10 females and (or) males from a given cross were measured to obtain the average for each genotype. Eye area measurements are consistent across independent experiments (Figure S1).

Thorax measurement

Thorax lengths (the distance from the base of the most anterior humeral bristle to the posterior tip of the scutellum) were measured using a Nikon SMZ-2B microscope equipped with a mechanical stage and a built-in micrometer.

Wing measurement

For each cross 5 healthy virgin females from both the dpp-Gal4 and the en-Gal4 stocks were mated with 5–10 healthy

males from w1118 (control), WT-24, and M-1 stocks. Flies of the appropriate genotype were incubated in 70% ethanol for at least 24 hr. Wings were mounted in Aqua PolyMount (Polysciences, Warrington, PA) on a glass slide. Only wings that had been flattened during the mounting process were used for further analysis. Images were captured using a Zeiss Axioscop microscope equipped with an AxioCam HRc camera and imported into ImageJ for analysis. Wing sizes in the case of the en-Gal4 driver were quantified by measuring the posterior area divided by total wing area. Wing sizes in the case of the dpp-Gal4 driver were quantified by measuring the area of sectors L4 and L3 area divided by the area of sectors L2–L4. Significance was determined by the Mann–Whitney *U*-test.

Bristle count

Three- to 5-day-old flies of the appropriate genotype (25 males and 25 females) were placed in Halocarbon 700 oil. The presence or absence of 26 bristles (macrochaetae; Figure S2) on the notum, including humeri, was scored.

Results

Transgene analysis

We generated transgenic flies carrying a single copy of either wild-type or mutant human preproinsulin (hINS^{WT} and hINS^{C96Y}, respectively), whose expression is regulated by a UAS:Gal4 promoter. A total of 27 independent transgenic stocks were produced, 8 carrying hINS^{WT} and 19 carrying hINS^{C96Y}, allowing us to investigate and control for position effects on gene expression. The hINS^{WT} lines also gave us the ability to identify mutation-dependent phenotypes in hINS^{C96Y} distinct from those resulting from both protein overexpression and/or interactions with native *Drosophila* insulin-like peptides (DILPs)-dependent pathways.

We investigated disease phenotypes by expressing transgenic hINS in imaginal discs of the eye (GMR-Gal4 driver), wing (en-Gal4 and dpp-Gal4 drivers), and notum (ap-Gal4 driver). The eye system was studied in greater detail than the others. GMR-Gal4 directs hINS transgene expression to developing photoreceptor neurons and surrounding support eye cells in the eye-morphogenetic furrow (http://flystocks.bio.indiana.edu/Reports/9146.html) (Freeman 1996). We confirmed transgene expression in F₁ adult heads by qRT-PCR (data not shown) and the presence of hINS protein in late third instar larval imaginal discs of GMR-Gal4/UAS-hINS^{C96Y} (or UAS-hINS^{WT}) individuals by immunofluorescent staining with an antibody specific for hINS C peptide (Figure 1, I–L).

We then examined the adult eye phenotypes caused by the mutant transgene expression in comparison to controls. Adult GMR-Gal4 flies and GMR-Gal4/UAS-hINS^{WT} flies from all 8 independent transgenic lines exhibited phenotypically wild-type eyes. In contrast, 11 of 19 independent transgenic lines of the mutant hINS (GMR-Gal4/UAS-hINS^{C96Y}) exhibited eye defects, including a reduction in eye area, a reduced number of eye bristles, the presence of lesions with no evidence of cells, and the collapse of ommatidial structure and normal array pattern.

The C96Y mutation is both necessary and sufficient to cause the eye degeneration phenotype. Insertion site position effect is known to influence transgene expression. We investigated whether the hINSWT lines might, by chance, be lower expressing than the hINSC96Y lines and for this reason not be exhibiting a defective eye phenotype. hINS transcript levels were quantified by qRT-PCR from total RNA of late third instar larval eye-imaginal discs from two mutant hINS lines, one exhibiting a mild eye phenotype (M-101) and the other a more severe eye phenotype (M-1), and from two wildtype hINS lines (WT-24 and WT-6), both of which exhibited wild-type eyes (Figure 2A). We did observe significant differences in transgene mRNA expression, but also found that WT-24 and M-1 expressed the transgenes at similar levels. We could reject, therefore, the formal possibility that the eye degeneration phenotype in the mutant is the result of gene expression alone: it requires mutant insulin. Moreover, a single copy of mutant hINS transgene (line M-1) is sufficient to cause eye degeneration (i.e., GMR-Gal4/UAS-hINS^{C96Y} or GMR>>hINSC96Y/CyO). Because mutant hINS line M-1 has a strong eye degeneration phenotype and the wild-type hINS control WT-24 expresses the transgene at a similar level, subsequent analyses were carried out, comparing these two lines.

The M-1 line exhibits a stronger eye degeneration phenotype than the M-101 line, and it expresses \sim 2.5 times more transcript in late third instar imaginal discs (Figure 2A). To further investigate the relationship between mutant hINS gene expression and the severity of disease, we set up crosses to manipulate gene dosage, allowing us to compare flies bearing either one or two copies of the hINSC96Y transgene and either one or two copies of the GMR-Gal4 driver transgene (Figure 3). The mutant phenotype is dramatically enhanced in double dose (w; GMR>>hINS^{C96Y}/GMR>>hINS^{C96Y}) compared to single dose (w; GMR>>hINSC96Y) and is more severe in males than in females. In contrast, GMR-Gal4 gene dose has no measurable effect on the severity of the eye degeneration phenotype in flies expressing one copy of hINS^{C96Y} and a small (but statistically significant) effect in flies carrying two doses of hINS^{C96Y}. All the subsequent experiments here and in an accompanying article in this issue (He et al. 2014) are with flies carrying a single copy of mutant hINS.

Eye phenotype

The adult eye in GMR-Gal4/UAS-hINS^{C96Y} flies display a number of characteristic defects, most notably a reduction in size. Individual ommatidia are often collapsed, lacking the wild-type organization of photoreceptor cells, giving the eye a glassy punctate phenotype (Figure 1, C and D). The regular array structure of ommatidia across the eye field is also disrupted, with the individual hairs projecting from each one either disarrayed or absent (Figure 1, G and H). Finally, black lesions can be present within the eye field where no cellular structure is evident (Figure 1, D and H).

The GMR-Gal4 driver activates expression in the cells posterior to the morphogenetic furrow in the eye discs (Freeman 1996). We therefore examined the organization

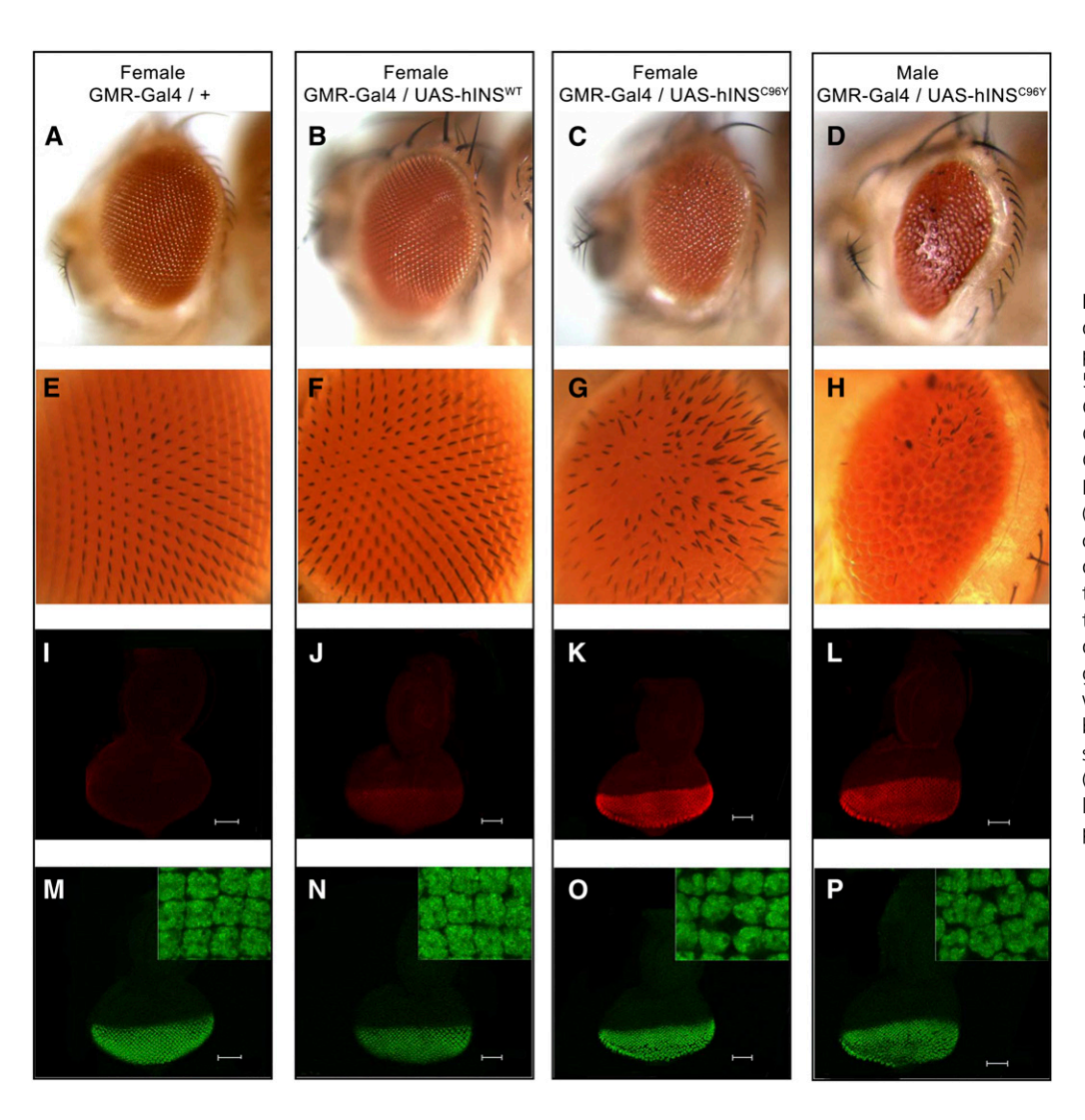


Figure 1 Eye phenotypes induced by hINSC96Y transgene expression. (A-D) Eyes of 3- to 5-day-old adults. (A) Female, GMR-Gal4. (B) Female, GMR-Gal4/UAS-hINSWT. (C) Female, GMR-Gal4/UAS-hINS^{C96}Y. Male, GMR-Gal4/UAS-hINS^{C96Y}. (E-H) High-magnification images of adult eyes in A-D showing defects in patterning of ommatidia and mechanosensory bristles. (I–L) Eye-antennal imaginal discs of third instar larvae of genotypes noted in A-D stained with anti-human C-peptide antibody (red). (M-P) Discs in I-L stained with anti-ELAV antibody (green). Insets in M-P show enlarged area of the most posterior part of the eye disc.

and cellular structure of developing ommatidia by costaining eye imaginal discs from wandering third instar larvae with anti-human C-peptide (a marker of proinsulin expression) (Park et al. 2010) and an antibody against ELAV, a neuron-specific RNA-binding protein widely used to stain rhabdomeres (Robinow and White 1991). This allowed us to confirm expression of wild-type and mutant proinsulin in the developing eye field (Figure 1, K and L). Ommatidial arrays at this early stage of eye formation are irregular and disorganized (Figure 1, O and P), indicating that the adult reduced-eye phenotype originates in the eye morphogenetic furrow with improper formation and maturation of photoreceptor cells, ommatidia, and ultimately the entire eye field.

The severity of the reduced-eye phenotype differs quantitatively between the two sexes. Mutant males in GMR-Gal4/UAS-hINS^{C96Y} flies exhibit a measurably stronger, *i.e.*, more degenerate, eye phenotype than females [Figure 1, C and G (female) *vs.* Figure 1, D and H (male)], a difference that is independent of gene dose, temperature, and genetic background (Carl 2010). This difference cannot be attributed to sex-specific difference in hINS expression, which does not differ significantly in the eye imaginal discs of either wild-

type or mutant hINS lines (Figure 2A). The male-biased phenotype, moreover, is not restricted to eye development; it is also observed in the notum and the wing when hINS^{C96Y} is expressed in the developing wing imaginal disc under the control of three other Gal4 drivers, as described below. The sex-biased phenotype appears to arise, therefore, not through tissue-specific development, but rather through a gender difference in cellular response to the mutant proinsulin protein.

Transcriptional profiles in eye imaginal discs expressing wild-type and mutant hINS

To investigate the effect of expressing hINS^{C96Y} on genome-wide transcription profiles and to identify the key changes in expression underlying the disease phenotype, we characterized gene expression profiles of RNA prepared from wandering third instar eye imaginal discs with the Affymetrix-GeneChip Drosophila Genome 2.0 Array. Imaginal discs were isolated from F_1 larvae carrying one copy of a GMR-Gal4 driver and one copy of either a wild-type or a mutant hINS transgene. As a control, we measured gene expression in a GMR-Gal4 \times w1118 cross. The experiments included two independent transgenic lines each for hINS^{WT} and hINS^{C96Y},

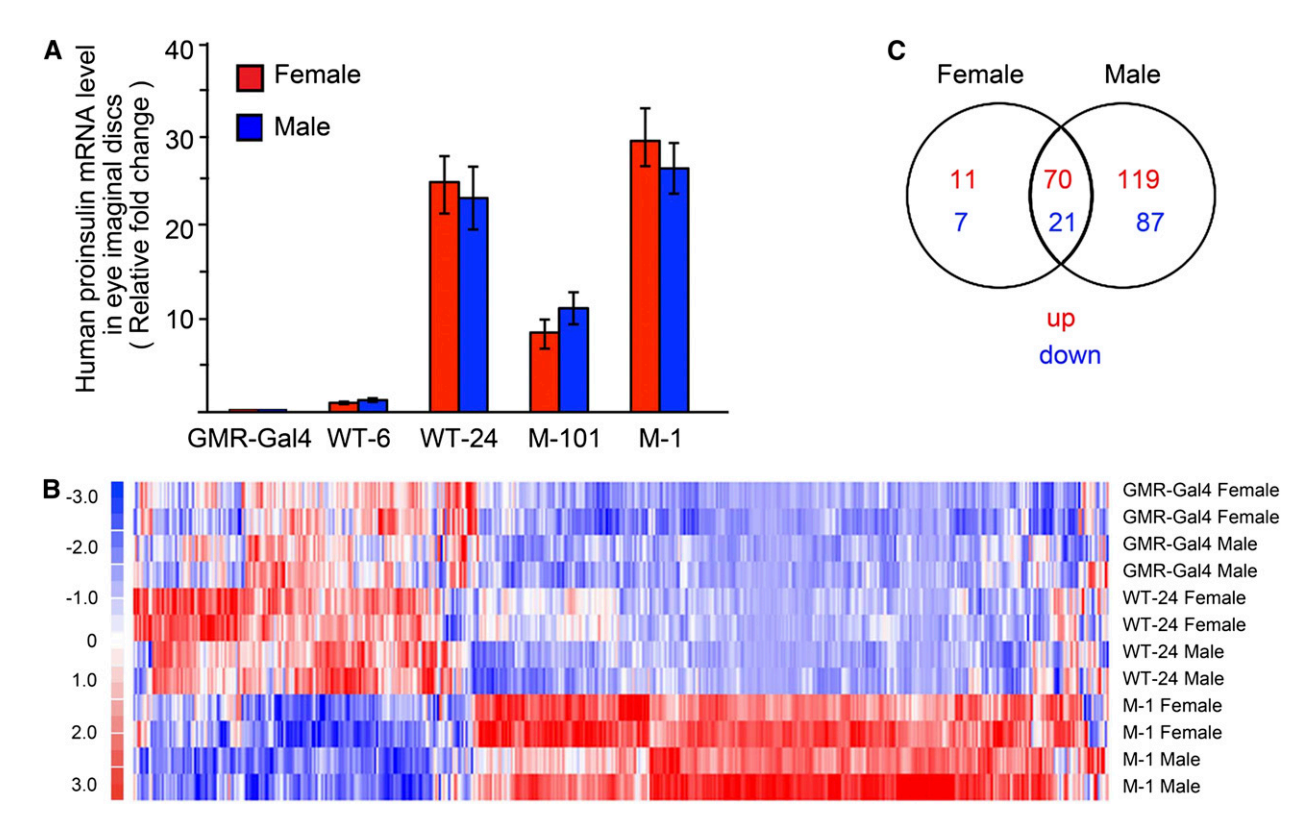


Figure 2 Gene expression in eye-antennal imaginal discs of third instar larvae. (A) Relative mRNA levels in discs from larvae expressing wild-type (WT) and mutant (M, hINS^{C96Y}) human proinsulin. WT-6, WT-24, M-101, and M-1 are independent transgenic lines. Gene expression is normalized to the expression level of rp49. The values (mean \pm SE) are shown relative to the ratio for female WT-6, set to one. (B) Heat maps of expression profiles in rows (genes) and columns (lines \times sex) for top 514 genes based on ANOVA between WT-24 and M-1 and the GMR-Gal4 control line are compared. ANOVA was performed for the three genotypes, two sexes, and two replicates according to the model $y = u + G + S + G \times S$, where G is the genotype and S is gender. Each gene was tested individually. A list of 514 genes was selected to control FDR < 5%. Each row is scaled to have mean 0 and variance 1. (C) Venn diagram showing the number of differentially expressed genes (up and down) in males and females in the comparison of WT-24 and M-1.

including the matched pair WT-24 and M-1 shown to express hINS mRNA at similarly high levels (Figure 2A). We first compared expression profiles between the GMR-Gal4 \times w1118 control and hINSWT- and hINSC96Y-expressing lines. After accounting for sex differences, we found no evidence for any effect on gene expression by wild-type hINS: there were no significant gene differences between the GMR-Gal4 control line and WT-6 and only a single difference in WT-24 at an FDR < 0.10 level (Figure S3). In contrast, 124 and 232 genes differed in males and females (respectively) between the mutant hINS lines and the GMR-Gal4 control. Thus, the effect on global gene expression caused by transgene expression can therefore be entirely attributed to the mutant proinsulin expression.

To visually illustrate the similarity and difference in gene expression between the control cross and hINS^{WT}-expressing and hINS^{C96Y}-expressing lines, we fitted an ANOVA model to each gene for three genotypes (GMR-Gal4 \times M-1; GMR-Gal4 \times WT-24; GMR-Gal4 \times w1118), accounting for sex effects (see *Data analysis 2* in *Materials and Methods*), in which we identified 514 probe sets with significant genotype differences (File S2). A heat map (Figure 2B) illustrates the similarities between the transcription profiles of hINS^{WT} and the control and confirms at the molecular level the lack of a visible phenotype caused by hINS^{WT} expression. It also

highlights the reorganization of transcription induced by hINS^{C96Y} expression.

We then analyzed differences in gene expression between GMR-Gal4 \times WT-24 and GMR-Gal4 \times M-1, because these two crosses had a matching, high level of expression of the transgenes. We found 297 genes whose expression differed in males (189 upregulated and 108 downregulated) and 109 genes that differed in females (81 upregulated and 28 downregulated) (Figure 2C; File S1). Of these, 91 overlapped between males and females (70 upregulated and 21 downregulated).

Inspection of the genes whose expression changed in response to mutant hINS revealed genes involved in protein folding/modification, protein degradation, and defense response/programmed cell death (Table 2; Table S2 and Table S3) and included representatives in UPR and ER-associated degradation (ERAD) pathways. An unbiased and unsupervised clustering analysis using David tools for Gene Ontology (GO) terms showed the greatest enrichment in membrane-bound proteins, while heat-shock proteins were also enriched (Table S4).

Although we did not observe a significant difference in the mRNA levels of the upstream regulators of the UPR [IRE1, PEK (PERK), Hsc70-3 (BiP; GRP78), and XBP1] in

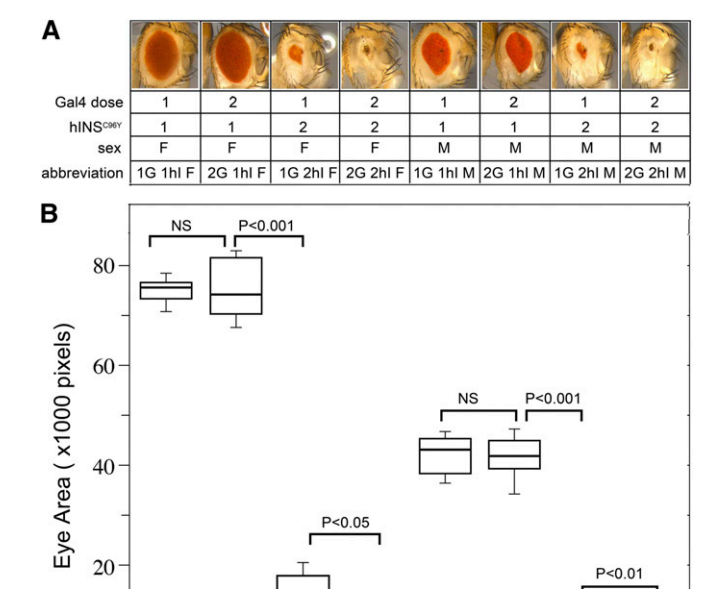


Figure 3 Eye degeneration in response to GMR-Gal4 and hINS^{C96Y} gene dose. The eye degeneration phenotype is much more sensitive to mutant insulin gene dose than to GMR-Gal4 dose. All four possible combinations of two-locus genotypes (one or two copies of either GMR-Gal4 or hINS^{C96Y}) were produced and adult eye areas measured separately for the two sexes, as described in *Materials and Methods*. (A) Representative adult eyes and the genotype abbreviations for the dosage series. (B) Box plot of eye area (*N* = 10 for each genotype/sex). Significance was determined by Student's two-tailed *t*-test. Genotype abbreviations: 1G 1hI [F, M]: w; GMR>>hINS^{C96Y} [Female, Male]; 2G 1hI [F, M]: w; GMR>>hINS^{C96Y}/UAS-hINS^{C96Y} [Female, Male]; 2G 2hI [F, M]: w; GMR>>hINS^{C96Y}/GMR>>hINS^{C96Y} [Female, Male].

the GeneChip analysis, a more sensitive analysis by qRT-PCR in male eye imaginal discs expressing mutant hINS compared to the GMR-Gal4 control revealed significant increases in expression of PERK (CG2087), BiP (CG4147), and XBP1 (CG9415) and a nearly significant increase in expression of IRE1 (CG4583; P = 0.08) (Table S5). As a more definitive test for activation of UPR, we also examined XBP1 mRNA for UPR-associated splicing by IRE1 and found evidence for it in mutant hINS-expressing cells but not in wild-type or GMR-Gal4-expressing cells (Figure S4). To confirm the microarray data by an independent method, we validated expression levels in the five lines (GMR-Gal4, WT-6, WT-24, M-101, and M-1) for five genes sets (CG3966, CG7130, CG10420, CG10160, and CG9150) whose expression was upregulated in males (Figure 2C). The results showed excellent correspondence between microarray and qRT-PCR (Table S6).

Expression of wild-type and mutant hINS in the notum and wing

Expression of mutant (but not wild-type) hINS in the notum, driven with an apterous driver (ap-Gal4), causes a reduction

in the posterior margin of the notum and a loss of macrochaetae (Figure 4, C and D). The adult fly notum has 22 macrochaetae (Figure S2), which in ap>>hINS^{C96Y} flies is reduced by an average of 8.3 and 13.4 bristles in females and males, respectively (Table S7). This 40% sex differential in bristle loss does not appear to be intrinsic to development—as a control we found no sex difference in bristle loss in the classic developmental mutant Scutoid (Sco) (Fuse *et al.* 1999), which suppresses notum bristles to approximately the same extent as mutant hINS expression, but does so to an equal extent in both sexes (Table S7).

Expression of mutant (but not wild-type) hINS in the developing wing imaginal disc causes visible defects in a proportion of adult wings (Figure 4, E-J). dpp-Gal4 drives expression in cells adjacent to the border of the posterior and anterior wing compartments; en-Gal4 drives expression only in the posterior wing compartment. In dpp-Gal4/UAShINS^{C96Y} flies, either the distal margins of ~30% of wings are scalloped or the anterior crossvein (ACV) is absent, both phenotypes being restricted to the domain where mutant proinsulin is predicted to be expressed. Expression of mutant hINS by the en-Gal4 driver results in occasional partial loss of ACV along its posterior boundary, also corresponding to the predicted region of mutant protein expression. Wing scalloping and ACV loss are striking phenocopies of the classical mutants Notch (incision of wing margin) and crossveinless, respectively, both regulators of wing development. Portions of the adult wing corresponding to mutant hINS expression in the wing imaginal disc are also significantly reduced in area (Figure 5).

Mechano-sensory structures on the wing—the campaniform sensillae—can also be absent in portions of the wing where mutant hINS is expressed under the control of the dpp- and en- drivers (Figure S5). One such sensilla lies along the anterior portion of the ACV and is typically absent when that portion of the crossvein is missing in en-Gal4/UAS-hINS^{C96Y} flies. In dpp-Gal4/UAS-hINS^{C96Y} flies, three additional sensillae sitting along the distal portion of the longitudinal wing vein 3 can also be absent (Table S8).

Mutant proinsulin expression in the developing wing also causes misspecification of cell fates to produce both ectopic wing veins and campaniform sensillae. The en-Gal4 driver, in particular, produces the novel appearance of both veins and sensillae (Figure 4J). A sensilla sitting along the ACV, when absent in en-Gal4/UAS-hINS^{C96Y} wings, is often replaced with an ectopic one appearing more anteriorly along the ACV or along the radial wing vein proximal to where it is intersected by the ACV. The posterior wing crossvein in the mutant can also project ectopic longitudinal veins.

hINS^{C96Y}-induced phenotypes are modified by genetic background

The eye, wing, and notum are notable examples of developmentally canalized structures that generally become more variable in a mutant background. Consistent with this observation, the mutant hINS-induced eye phenotype

Table 2 Selected genes upregulated by GMR-Gal4/UAS-hINSC96Y in male eye imaginal discs

Probe set	Transcript	Name	Description (GO) ^a	Homolog ^b
Protein modification/folding				
1639033_at ^c	CG9432-RB	l(2)01289	Disulfide isomerase	
1623862_at ^c	CG3966-RA	ninaA	HSP ^d	
1628660_at ^c	CG7130-RA	CG7130	HSP ^d binding	DNAJB1
1623247_at ^c	CG10420-RA	CG10420	HSP ^d	SIL1
1627525_a_at	CG1333-RA	Ero1L	Thiol-disulfide exchange	ERO1LB
1641511_at	CG7394-RA	TIM14	HSP ^d binding	DNAJC19
1641563_at	CG8286-RA	P58IPK	HSP ^d binding	DNAJC3
1634528_at	CG8412-RA	CG8412	Glycosyltransferase	ALG12
1638456_at	CG8531-RA	CG8531	HSP ^d binding	
Protein degradation				
1632071_at	CG8870-RA	CG8870	Serine-type endopeptidase activity	
1637515_s_at ^c	CG1512-RA	Cullin-2	Ubiquitin-protein ligase	CUL2
1626272_s_at ^c	CG3066-RA	Sp 7	Peptidase	SP7
1626460_at	CG2658-RA	CG2658	Peptidase	SPG7
1635051_a_at	CG14536-RA	Herp	Ubiquitin-protein ligase	HERPUD2
1634486_at	CG30047-RA	CG30047	Peptidase	
1624372_at	CG10908-RA	Derlin-1	Peptidase	DERL1
1637955_a_at ^c	CG1827-RA	CG1827	Lysosome	
1625253_at	CG4909-RA	POSH	Ubiquitin-protein ligase	SH3RF1
1623029_at	CG31535-RA	CG31535	Ubiquitin-protein ligase	
1634899_a_at	CG6512-RA	CG6512	Peptidase	AFG3L2
Defense response/programmed	d cell death			
1636668_at	CG9972-RA	CG9972	Apoptosis ^e	
1624450_at	CG6331-RA	Orct	Apoptotic process	
1633145_at	CG4437-RA	PGRP-LF	Apoptosis ^e	PGLYRP3
1622979_a_at	CG7188-RB	Bax inhibitor-1	Apoptosis ^e	
1641298_at	CG10535-RA	Elp1	Defense response	
1634714_at	CG1676-RA	Cactin	Defense response	C19orf29
1635028_s_at	CG33047-RA	Fuca	Defense response	FUCA2
1638100_s_at	CG1228-RD	Ptpmeg	Apoptotic process	PTPN4
1628174_at	CG33119-RA	nim B1	Defense response	

^a GO molecular function/process from http://www.flybase.org, www.uniprot.org, and http://david.abcc.ncifcrf.gov.

displays sensitivity to temperature and differs between the two sexes. In crosses involving the third chromosome balancer TM3, we also observed more severe eye phenotypes when the balancer chromosome was present (Carl 2010), indicating sensitivity to the genetic background. We therefore examined the extent to which naturally occurring genetic variation modifies the mutant hINS phenotype in the eye and notum. We crossed a tester stock carrying the mutant transgene (M-1) and either the GMR-Gal4 or ap-Gal4 driver on the same second chromosome (GMR>>hINSC96Y or ap>>hINSC96Y) with 38 reference inbred lines derived from a single population collection, the DGRP (Mackay et al. 2012), and measured eve phenotypes or counted dorsal macrochaetae in F₁ adults. The F₁ males in the crosses carried an identical X chromosome—the tester chromosome. The screen, therefore, revealed only partially or fully dominant autosomal modifiers of the mutant phenotype. For each cross we measured eye area or dorsal bristle number in a minimum of 10 individuals of each sex.

Eye phenotypes: The crosses revealed highly heritable genetic variation [h^2 (males) = 0.732; h^2 (females) = 0.657], visible as a nearly continuous distribution of between-line differences

in eye degeneration phenotypes, ranging from nearly wild-type to highly reduced and slit-like eyes (Figure 6, A and C). These interline differences are not correlated with each line's body size [bivariate fit of eye area with thorax length, $r^2 = 0.0051$ (Carl 2010)] or eye area (Figure S6) or with the quantity of Gal4 protein, which did not vary significantly (Figure S7). There are also significant between-line differences in other aspects of the eye phenotype, including aspect ratio (width:height), ommatidial degeneration, and prevalence of lesions (Carl 2010). Lesion prevalence, unlike aspect ratio or ommatidial degeneration, was not significantly correlated with the extent of eye loss ($r^2 = 0.01$), indicating the two have independent genetic underpinnings rather than being the consequence of pleiotropy.

Notum phenotypes: As with the eye phenotype, we found significant interline variation ranging from lines with nearly wild-type bristle number (RAL-427, 25.6 \pm 0.7) to ones missing a majority of bristles (RAL-335, 11.0 \pm 1.1) and with a high heritability [h^2 (males) = 0.744] (Figure 6D; Table S11).

^b Human homolog from http://flight.icr.ac.uk.

^c Upregulated in female and male.

^d Heat-shock protein.

^e Negative regulation.

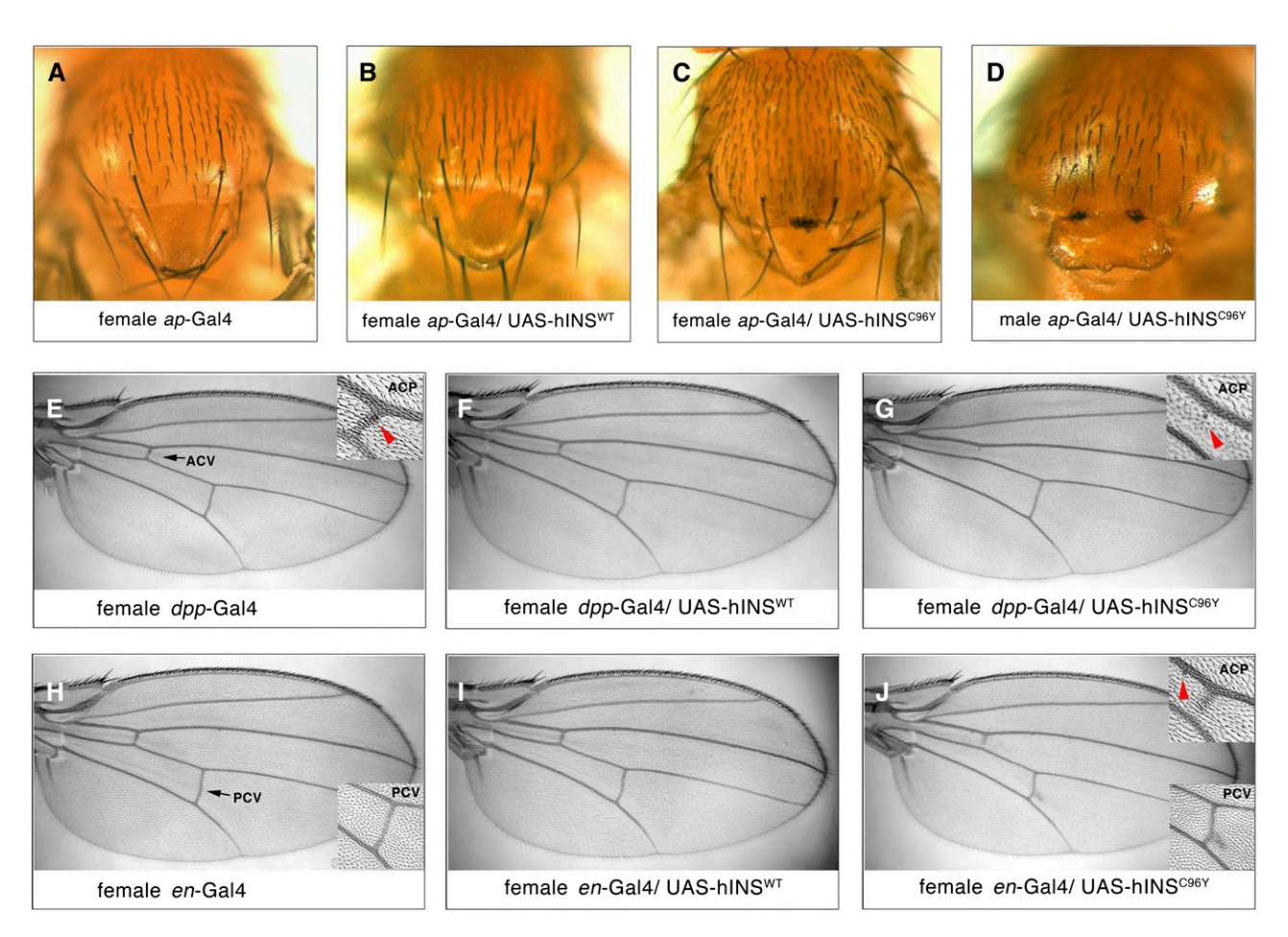


Figure 4 Notum and wing phenotypes induced by hINS^{C96Y} transgene expression. (A–J) Notum (A–D) and wing (E–J) phenotypes in 3- to 5-day-old adults of indicated sex and genotype. Insets show a higher-magnification view of the anterior or posterior crossvein (ACV) with the *campaniform sensillae* shown by an arrow. Note the missing anterior crossvein in G (dpp-Gal4 driver), the partial anterior crossvein and abnormal posterior crossvein in J (en-Gal4 driver), and the relocation of the *companiform sensillae* from the anterior crossvein to the longitudinal vein in J.

Disease traits are uncorrelated

We reasoned that if the genetic pathways responding to hINS^{C96Y} expression common to both eye and notum, such as UPR, harbor modifiers of the response, then the severity of the eye reduction and bristle loss should be positively correlated in the sample of DGRP lines. To ask whether the same modifiers are acting in a similar manner in both tissues we measured the correlation between traits in the 38 lines for which both were measured. Surprisingly, we found no evidence for a positive correlation (Figure 6E; Table S9; male, Spearman's rank correlation $\rho = -0.23$, P = 0.16; female, $\rho = -0.17$, P = 0.30). Either the common response pathways harbor little of the genetic variation for the disease phenotypes or their penetrance must be modulated by tissue-specific factors.

Variation in eye-specific genetic pathways is uncorrelated with hINS^{C96Y}-induced phenotypes

The lack of correlated mutant hINS-induced phenotypes in the eye and notum raises an alternative possibility that genetic variation acts not through shared response pathways but rather through tissue-specific developmental pathways and in so doing "releases" pathway-specific genetic variation otherwise suppressed in the wild type. To test this possibility, we examined genetic variation in the DGRP lines for two eye-development-specific genetic mutations, Lobe (L) and Drop (Dr). L and Dr are classic dominant eye-degeneration mutations that can be crossed to the DGRP lines in the same manner as the mutant proinsulin transgene to reveal dominant genetic variation for reduced-eye phenotypes. L encodes the ortholog of mammalian PRAS40 and regulates eye development through TORC1 signaling (Wang and Huang 2009); mutants display an apoptotic reduced-eye phenotype. L acts through the Jak/Stat signaling pathway in the ventral eye, possibly interacting with the *Notch* ligand, Serrate (Chern and Choi 2002). Dr, in contrast, is a muscle segment homeobox-1 (msh) transcription factor that regulates interaction between epithelial and mesenchymal cells. It is active in embryonic neural dorsal-ventral patterning and again in eye development. Dr mutants ectopically express msh, blocking morphogenetic furrow progression in the developing eye, leading to apoptotic photoreceptor cell loss and a nearly eyeless phenotype (Mozer 2001).

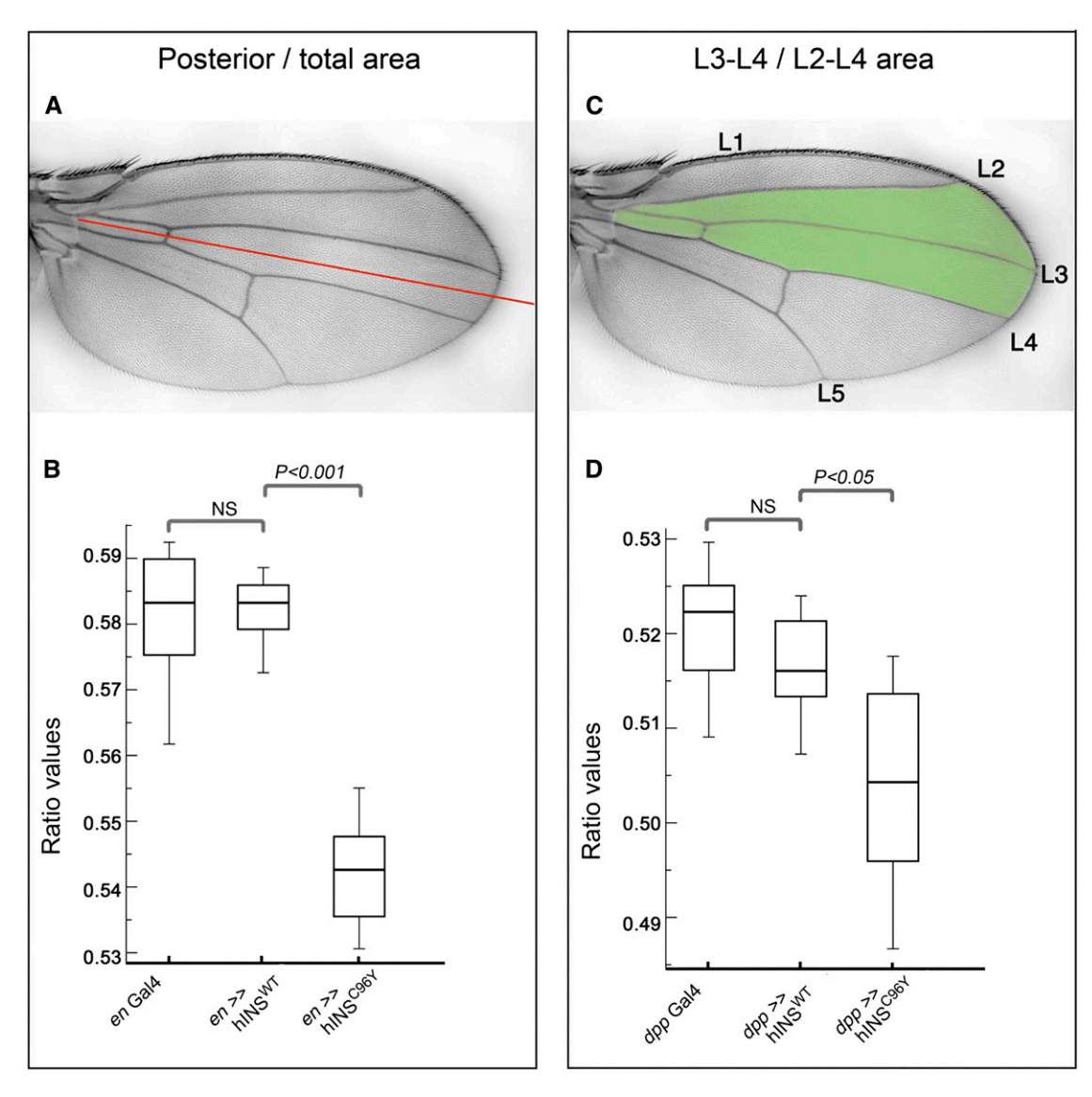


Figure 5 Expression of hINS^{C96Y} in different compartments produces a nonallometric reduction in wing size. (A and C) Control wings showing the regions used to quantify the effects of hINS^{C96Y} expression. The red line denotes the border between the anterior (above) and posterior (below) compartments of the wing. en-GAL4 expresses in the posterior compartment. The five longitudinal wing veins are labeled L1–L5. The L2–L4 intervein sector is shadowed in green. dpp-GAL4 expresses in the L3–L4 intervein sector. (B) en genotypes: en-Gal4 (n = 13), en-Ga4/UAS-hINS^{WT} (n = 13), and en-Gal4/UAS-hINS^{C96Y} (n = 13). Values represent the ratio of the posterior wing compartment divided by the total wing area. (D) dpp genotypes: dpp-Gal4 (n = 10), dpp-Gal4/UAS-hINS^{WT} (n = 10), and dpp-Gal4/UAS-hINS^{C96Y} (n = 11). Values represent the ratio of the L3–L4 intervein sector divided by the L2–L4 intervein sector area. NS, not significant, Mann–Whitney n = 11.

The genetic variation exposed by mutant hINS expression appears to be distinct from the genetic variation exposed by eye development mutants despite its apparent tissue specificity. We crossed L, Dr, and hINS^{C96Y} to 38 DGRP lines and collected F_1 adults for eye area measurement. Variation in hINS^{C96Y}-induced eye degeneration was comparable to previous measurements in the same lines (Figure 7, A and D; Figure S1 and Figure S8; Table S10 and Table S11). F_1 flies displayed heritable variation for both Dr and L phenotypes, which when scaled by their within-line variances displayed a range of phenotypes similar to hINS^{C96Y} flies (Figure 7, A and B). There is no significant correlation between any pair of traits (Figure 7C; Table S9) and thus no evidence for

shared variation acting on mutant hINS and two eyedevelopment-specific mutants. It is also worth noting that for both L and Dr, eye area in males is \sim 85% that of females, consistent with the difference in wild-type flies. In contrast, eye area in males of mutant proinsulin-expressing crosses is 50% that of females, indicating a sex-specific input to the disease phenotype (also see Figure 6, C and D).

Discussion

Drosophila is a useful model for studying cell function and development in response to misfolded proinsulin. We show that mutant (but not wild-type) hINS expression causes

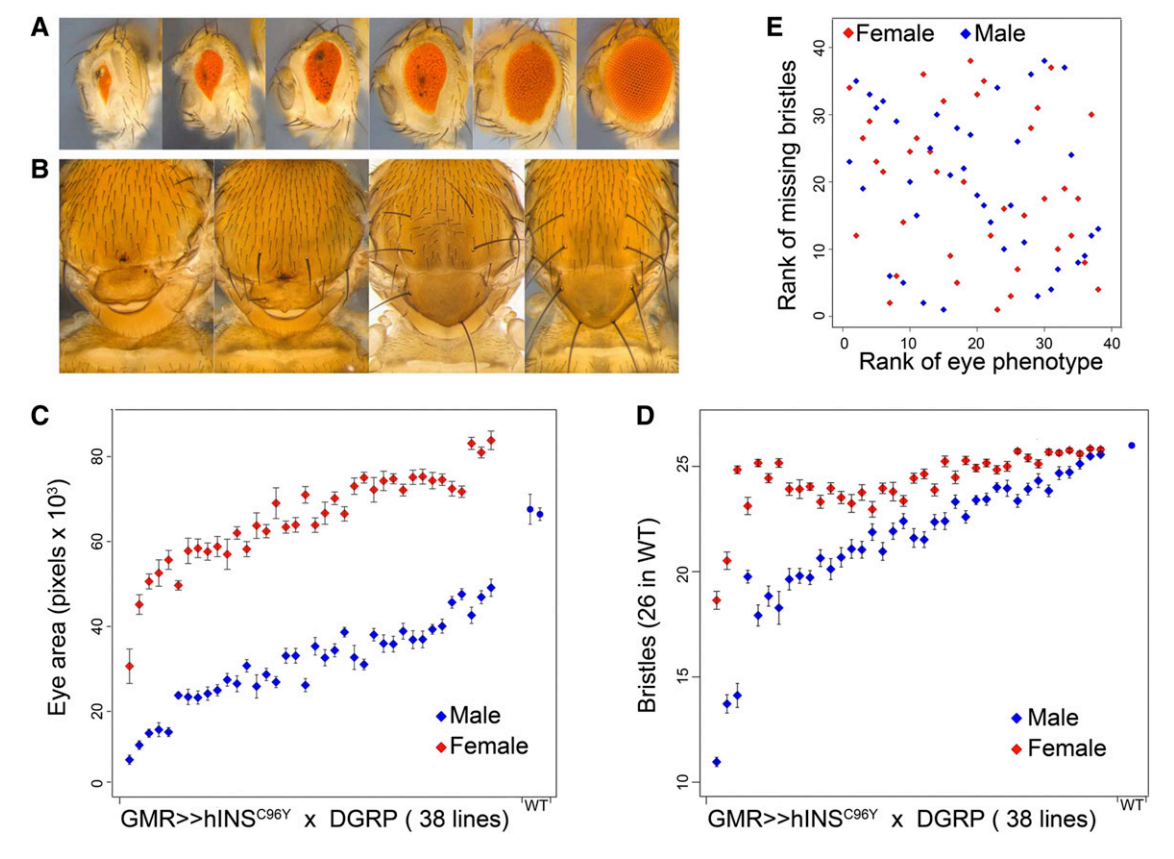


Figure 6 Genetic variation for hINS^{C96Y}-induced degeneration in the adult eye and notum. (A) Variation in eye area in F_1 adults from crosses between the GMR>>hINS^{C96Y} tester strain and 38 DGRP lines described in *Materials and Methods*. (B) Bristle number in F_1 adults from crosses in A. (C and D) Eye area and bristle number. The data are displayed from left to right by decreasing severity of phenotypes. Eye area (mean \pm SE) for a wild-type control (GMR-Gal4 \times w1118) is shown on the far right in solid circles (in C, only male wild-type eye areas are shown). (E) Correlation between bristle loss and eye area reduction (male, Spearman's rank correlation $\rho = -0.23$, P = 0.16; female, $\rho = -0.17$, P = 0.30).

a reduction in size (and cell number for eyes) in every tissue examined. Human proinsulin is not processed to insulin in developing eye cells, but can be induced to do so by overexpressing a secretory cell master regulator, the bHLH transcription factor DIMMED (Park et al. 2012). Consistent with this result, we observed no effect of wild-type hINS expression on gene expression or eye development. Although we have not established a specific mechanism (or mechanisms) by which mutant-induced eye reduction occurs, one of them is likely to involve UPR, which we show is induced based on both the presence of XBP1 alternatively spliced mRNA in eye imaginal discs expressing hINSC96Y and the induction of well-known stress response genes, including those aiding protein folding and promoting programmed cell death. We also establish a reorganization of gene expression in imaginal disc cells in response to mutant hINS expression.

Cell death in the *Drosophila* model recapitulates a key feature of disease observed in mouse diabetes caused by the same C96Y mutation in *Ins2*: the dominant loss of insulin-secreting β -cells (Kayo and Koizumi 1998; Wang *et al.* 1999). In the mouse model, the synthesis of misfolded proinsulin leads to its retention in the ER, resulting in induction of UPR, death of the insulin-secreting pancreatic β -cells, and diabetes (Song *et al.* 2008; Tabas and Ron

2011). The human form of hINS^{C96Y}-induced disease is believed to act through the same mechanism (Liu *et al.* 2010; Park *et al.* 2010); based on our gene expression experiment, this may hold true in the *Drosophila* model as well.

Developing tissues, we discovered, are more sensitive to mutant hINS expression in males than in females. When expressed in the eye, hINSC96Y causes a nearly twofold reduction in eye area in males compared to females. Other features of the eye, including the presence of necrotic lesions, photoreceptor cell collapse, and ommatidial disorganization, are also more evident in males, L and Dr in contrast, although also producing reduced-eye phenotypes, do not exhibit sex-specific differences relative to wild type. The flexibility of the *Drosophila* model allowed us to establish that the notum also displays a differential male sensitivity to mutant hINS expression. We believe, therefore, that the greater sensitivity to mutant hINS in males must involve cell physiology rather than tissue-specific development. We can entertain at least two hypotheses for the male sensitivity, both of which are potentially testable. One obvious possibility involves disruption of dosage compensation. In Drosophila, dosage compensation occurs in males by upregulating X-linked genes through the activity of the male sex-lethal (MSL) complex (Gelbart and Kuroda 2009). Reorganization

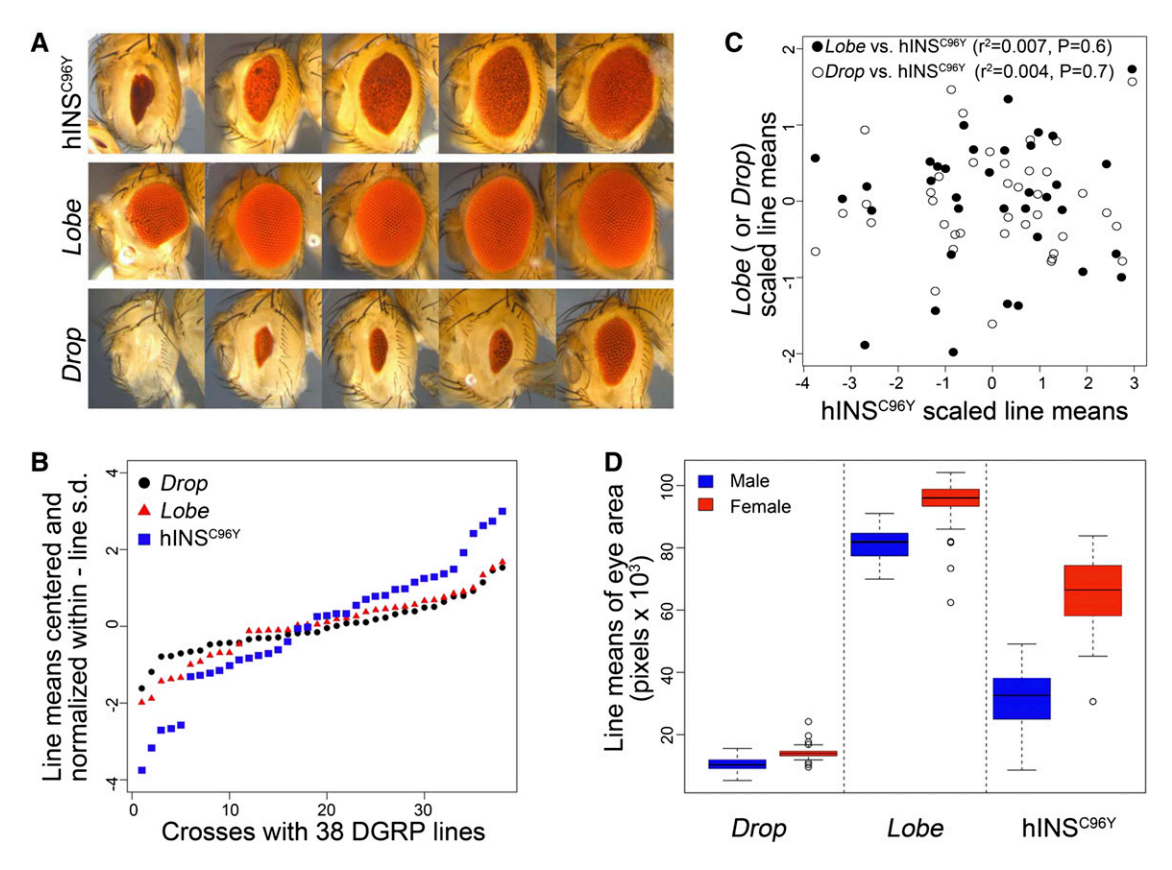


Figure 7 Genetic variation for eye area reduction in F_1 adults from crosses between GMR>>hINS^{C96Y}, *Drop*, or *Lobe* and 38 DGRP lines. (A) Range of phenotypes in F_1 adults in both sexes. (B) Deviation (in units of within-line SD) of each line mean from the overall mean within each of the three sets of crosses. (C) Correlation of eye area reduction between hINS^{C96Y} and *Dr* (open circles) or *L* (solid circles) \times DGRP F_1 males. (D) Box plots showing the unscaled distribution of phenotypes in the three sets of crosses [thick line, median; box, 25th and 75th percentiles; whisker, 1.5 interquartile range (IQR); circles, data outside the 1.5 IQR].

of gene expression in stressed cells may disrupt maintenance of dosage compensation, leading to the exacerbation of cellular stress and cell death in males. An alternative hypothesis posits that cells in males are less well canalized against perturbation, such as with expression of mutant hINS, perhaps because dosage compensation introduces greater variability in X-linked gene expression. It is well known, for example, that the effectiveness of dosage compensation varies quantitatively across X-linked genes and is complete in only a subset of them (Hamada et al. 2005). Cell-to-cell or temporal variation in X-linked gene expression might increase demand on the homeostatic mechanisms involving proteostasis. It should be possible to test these hypotheses by genetically manipulating flies to examine sex determination, dosage compensation, or sex differentiation pathway contributions to male-biased disease. More generally, fly models of human disease, such as ours, may be valuable in disentangling environmental and genetic contributions to sex differences in susceptibility or severity of disease, a notoriously difficult problem in human studies.

Male sex bias may be a general property of the disease: it is also a feature of diabetes in mice (Wang *et al.* 1999). Male mice heterozygous for $Ins2^{C96Y}$ develop diabetes at an earlier age than females (Oyadomari *et al.* 2002). In the fly,

X-linked genes are upregulated in males whereas in mammals a single X chromosome is inactivated in female cells. If the mechanism underlying the male bias in fly and mouse is the same, it is unlikely, therefore, to directly involve dosage compensation.

A second unexpected finding was the presence of fully differentiated ectopic veins and sensory structures in wings expressing mutant hINS. These same wings also display loss-of-structure phenotypes, including crossveins and campaniform sensillae, as well as scalloping of wing margins. Both ectopic gain and loss of these differentiated tissues are striking phenocopies of classical wing mutations, many of which have been shown to be involved in the regulation of wing development (Neto-Silva et al. 2009). We believe, therefore, that mutant hINS expression can not only induce cell death, but also lead to reprogramming of cell fates. An interesting implication for the human form of the disease is that loss of β -cells in neonates may involve not only cell death but also transformation of precursor cells to other cell types.

Third, crosses to a reference panel of naturally derived lines (DGRP) revealed extensive dominant (or partially dominant) genetic variation acting to suppress or enhance cell loss. One possibility, which we investigated and could reject, is variation in mutant hINS gene expression in different DGRP backgrounds. Since all the flies carry the same tester chromosome (GMR $>>hINS^{C96Y}$), we focused our attention on Gal4 instead, because its expression could be influenced by variation in transcription factors acting on its promoter, GMR; we found no evidence for differences in Gal4 protein levels between DGRP lines representative of the full range of eye degeneration phenotypes (Figure S7). GMR is a synthetic enhancer consisting of binding sites for the eye-specific transcription factor glass (gl). In an accompanying article, we also find no evidence for association of genetic variation in or around the gl locus with eye degeneration (He et al. 2014). We do not believe, therefore, that variation in eye degeneration is caused by genetic variation in the transcription of mutant hINS.

Finding extensive genetic variation in eye degeneration in our F_1 screen establishes the feasibility of applying methods of statistical association to identify modifiers of disease, the subject of the accompanying article (He *et al.* 2014). Here we explored other dimensions of this variability. It is worth noting that many, if not most, Mendelian models of disease in the fly involve gain-of-function alleles, which facilitates screens for natural variation in F_1 flies. In addition to the convenience of this genetic screen, it also eliminates phenotypes resulting from the homozygosity of deleterious alleles in inbred lines. Outcrossed genotypes are well suited for investigating low-frequency variants, which are rarely homozygous in natural populations.

Disease phenotypes in the eye and notum were not significantly correlated in the DGRP panel, suggesting that different suites of alleles are acting in the two tissues. A positive correlation would be expected if genetic variation occurred primarily in shared pathways responding to mutant hINS expression, such as UPR. Not finding evidence for such a correlation, we then investigated whether a correlation would be observed when comparing a single phenotype—eye reduction—caused by hINS and by two classical mutations, L and Dr. The fact that we failed to find significant correlations between either L or Dr and hINS^{C96Y} leaves us with a puzzling set of results: natural variation for hINS-induced disease severity exhibits tissue specificity but involves a different set of genes or alleles than the ones revealed with eye-developmentspecific mutants. The latter result, but perhaps not the former, should come as no surprise. In other models of Mendelian disease, e.g., aggregation-prone proteins expressed in the developing eye, forward genetic screens for suppressors and enhancers of reduced eye phenotypes successfully identify genes acting in pathways known to be responsive to proteostatic stress: UPR, apoptosis, RNA-folding, peptidefolding, transit, and degradation pathways (Chai et al. 1999; Warrick et al. 1999, 2005; Chan et al. 2000; Chan and Bonini 2003; Bilen and Bonini 2005, 2007; Lessing and Bonini 2008; Li et al. 2008; Yu and Bonini 2011), but not regulators of eye development. As this also appears to be the case for naturally occurring variation in our Mendelian model of disease, distinct alleles and genes must be acting as modifiers, perhaps epistatically, in different tissues.

An alternative hypothesis can be constructed on the premise that the spectrum of mutations affecting this complex disease trait may have a much broader set of targets, needing only to impinge on processes involved in cellular or physiological homeostasis. Disease occurs when an individual's homeostatic "capacitance"—the ability to buffer against cellular stress—is exceeded. Whether a threshold is crossed will depend on both the cellular activities set by an individual's background genotype and the environmental demands or rare mutant alleles acting critical pathways.

Subtle effects of genetic background on the ability of a cell to balance protein synthesis, folding, transport, and degradation—*i.e.*, proteostasis—may be responsible for many diseases, in addition to diabetes. Under this hypothesis, a complex and diffuse web of interacting polymorphisms sets an individual's ability to respond to genetic or environmental challenges, determining susceptibility to and severity of disease. If true, the vast majority of mutations and the spectrum of disease-causing loci segregating in natural populations are likely to be systematically and substantially different from the strong loss- or gain-of-function alleles identified in forward genetic screens alone.

In addition, as proteomes differ between tissues, so too will the alleles affecting proteostasis. This possibility is illustrated by revealing experiments on two aggregation-prone/misfolded proteins in a worm model: polyglutamine protein (Gidalevitz *et al.* 2006) and mutant SOD1 (Gidalevitz *et al.* 2009). In both cases, temperature-sensitive (*ts*) mutations in housekeeping proteins, although innocuous when the worm is reared below the *ts* threshold, enhance mutant protein phenotypes, and hence toxicity, when the *ts* threshold is exceeded. SOD1 phenotypes are also sensitive to the genetic background.

Drosophila is an excellent model for investigating naturally occurring genetic variation for quantitative traits. The recent establishment of the DGRP (Mackay et al. 2012), of synthetic populations (Huang et al. 2012; King et al. 2012), and of other novel population resequencing approaches (Turner and Miller 2012) adds to its power and appeal. Here we extend the applicability of these approaches to the study of human disease. An important question remaining to be addressed is whether the extensive genetic variation revealed in this study of a genetically "sensitized" fly is the same as the variation underlying complex genetic forms of the disease, an issue further discussed in the accompanying article (He et al. 2014). An affirmative answer to this question raises the prospect for using Drosophila as a model of genetically complex human disease.

Acknowledgments

We thank Honggang Ye, Esme Gaisford, Amanda Neisch, Richard Morimoto, Ilya Ruvinsky, Richard Hudson, Rick Fehon, and Ilaria Rebay for technical help and advice. This work was funded by grants from the National Institute of Diabetes and Digestive and Kidney Diseases (R01DK013914)

and P30DK020595), the National Institute of General Medical Sciences (P50GM081892), and the Chicago Biomedical Consortium with support from the Searle Funds at The Chicago Community Trust and by a gift from the Kovler Family Foundation. The content is solely the responsibility of the authors and does not necessarily represent the official views of the National Institute of Diabetes and Digestive and Kidney Diseases, the National Institute of General Medical Sciences, or the National Institutes of Health.

Note added in proof: See He *et al.* 2014 (pp. 557–567) in this issue for a related work.

Literature Cited

- Ayroles, J. F., M. A. Carbone, E. A. Stone, K. W. Jordan, R. F. Lyman et al., 2009 Systems genetics of complex traits in Drosophila melanogaster. Nat. Genet. 41: 299–307.
- Bedell, M. A., N. A. Jenkins, and N. G. Copeland, 1997a Mouse models of human disease. Part I: techniques and resources for genetic analysis in mice. Genes Dev. 11: 1–10.
- Bedell, M. A., D. A. Largaespada, N. A. Jenkins, and N. G. Copeland,1997b Mouse models of human disease. Part II: recent progress and future directions. Genes Dev. 11: 11–43.
- Bell, G. I., W. F. Swain, R. Pictet, B. Cordell, H. M. Goodman et al., 1979 Nucleotide sequence of a cDNA clone encoding human preproinsulin. Nature 282: 525–527.
- Benjamini, Y., and Y. Hochberg, 1995 Controlling the false discovery rate: a practical and powerful approach to multiple testing. J Roy. Statist. Soc. Ser. B 57: 289–300.
- Bergland, A. O., A. Genissel, S. V. Nuzhdin, and M. Tatar, 2008 Quantitative trait loci affecting phenotypic plasticity and the allometric relationship of ovariole number and thorax length in *Drosophila melanogaster*. Genetics 180: 567–582.
- Bilen, J., and N. M. Bonini, 2005 Drosophila as a model for human neurodegenerative disease. Annu. Rev. Genet. 39: 153–171.
- Bilen, J., and N. M. Bonini, 2007 Genome-wide screen for modifiers of ataxin-3 neurodegeneration in Drosophila. PLoS Genet. 3: 1950–1964.
- Biteau, B., J. Karpac, D. Hwangbo, and H. Jasper, 2011 Regulation of Drosophila lifespan by JNK signaling. Exp. Gerontol. 46: 349–354.
- Carl, S. H., 2010 Naturally occurring genetic variation influences the severity of Drosophila eye degeneration induced by expression of a mutant human insulin gene. Undergraduate Thesis, University of Chicago, Chicago.
- Chai, Y., S. L. Koppenhafer, N. M. Bonini, and H. L. Paulson, 1999 Analysis of the role of heat shock protein (Hsp) molecular chaperones in polyglutamine disease. J. Neurosci. 19: 10338–10347.
- Chan, H. Y., and N. M. Bonini, 2003 Drosophila models of polyglutamine diseases. Methods Mol. Biol. 217: 241–251.
- Chan, H. Y., J. M. Warrick, G. L. Gray-Board, H. L. Paulson, and N. M. Bonini, 2000 Mechanisms of chaperone suppression of polyglutamine disease: selectivity, synergy and modulation of protein solubility in Drosophila. Hum. Mol. Genet. 9: 2811–2820.
- Chern, J. J., and K. W. Choi, 2002 Lobe mediates Notch signaling to control domain-specific growth in the Drosophila eye disc. Development 129: 4005–4013.
- Chintapalli, V. R., J. Wang, and J. A. Dow, 2007 Using FlyAtlas to identify better Drosophila melanogaster models of human disease. Nat. Genet. 39: 715–720.
- Cox, J. S., and P. Walter, 1996 A novel mechanism for regulating activity of a transcription factor that controls the unfolded protein response. Cell 87: 391–404.

- Dworkin, I., and G. Gibson, 2006 Epidermal growth factor receptor and transforming growth factor-beta signaling contributes to variation for wing shape in *Drosophila melanogaster*. Genetics 173: 1417–1431.
- Dworkin, I., E. Kennerly, D. Tack, J. Hutchinson, J. Brown et al., 2009 Genomic consequences of background effects on scalloped mutant expressivity in the wing of *Drosophila mela*nogaster. Genetics 181: 1065–1076.
- Freeman, M., 1996 Reiterative use of the EGF receptor triggers differentiation of all cell types in the Drosophila eye. Cell 87: 651–660.
- Fuse, N., H. Matakatsu, M. Taniguchi, and S. Hayashi, 1999 Snailtype zinc finger proteins prevent neurogenesis in Scutoid and transgenic animals of Drosophila. Dev. Genes Evol. 209: 573–580.
- Gelbart, M. E., and M. I. Kuroda, 2009 Drosophila dosage compensation: a complex voyage to the X chromosome. Development 136: 1399–1410.
- Geminard, C., E. J. Rulifson, and P. Leopold, 2009 Remote control of insulin secretion by fat cells in Drosophila. Cell Metab. 10: 199–207.
- Gibson, G., and L. K. Reed, 2008 Cryptic genetic variation. Curr. Biol. 18: R989–R990.
- Gidalevitz, T., A. Ben-Zvi, K. H. Ho, H. R. Brignull, and R. I. Morimoto, 2006 Progressive disruption of cellular protein folding in models of polyglutamine diseases. Science 311: 1471–1474.
- Gidalevitz, T., T. Krupinski, S. Garcia, and R. I. Morimoto, 2009 Destabilizing protein polymorphisms in the genetic background direct phenotypic expression of mutant SOD1 toxicity. PLoS Genet. 5: e1000399.
- Goering, L. M., P. K. Hunt, C. Heighington, C. Busick, P. S. Pennings et al., 2009 Association of orthodenticle with natural variation for early embryonic patterning in Drosophila melanogaster. J. Exp. Zool. B Mol. Dev. Evol. 312: 841–854.
- Hamada, F. N., P. J. Park, P. R. Gordadze, and M. I. Kuroda, 2005 Global regulation of X chromosomal genes by the MSL complex in Drosophila melanogaster. Genes Dev. 19: 2289–2294.
- Hartley, T., M. Siva, E. Lai, T. Teodoro, L. Zhang et al., 2010 Endoplasmic reticulum stress response in an INS-1 pancreatic beta-cell line with inducible expression of a folding-deficient proinsulin. BMC Cell Biol. 11: 59.
- Haselton, A. T., and Y. W. Fridell, 2010 Adult Drosophila melanogaster as a model for the study of glucose homeostasis. Aging 2: 523–526.
- He, B. Z., and M. Z. Ludwig, D. A. Dickerson, L. Barse, B. Arunet al., 2014 Effect of genetic variation in a *Drosophila* model of diabetes-associated misfolded human proinsulin. Genetics 196: 557–567.
- Huang, W., S. Richards, M. A. Carbone, D. Zhu, R. R. Anholt et al., 2012 Epistasis dominates the genetic architecture of *Drosophila* quantitative traits. Proc. Natl. Acad. Sci. USA 109: 15553–15559.
- Kang, M. J., and H. D. Ryoo, 2009 Suppression of retinal degeneration in Drosophila by stimulation of ER-associated degradation. Proc. Natl. Acad. Sci. USA 106: 17043–17048.
- Kang, M. J., J. Chung, and H. D. Ryoo, 2012 CDK5 and MEKK1 mediate pro-apoptotic signalling following endoplasmic reticulum stress in an autosomal dominant retinitis pigmentosa model. Nat. Cell Biol. 14: 409–415.
- Karpac, J., and H. Jasper, 2009 Insulin and JNK: optimizing metabolic homeostasis and lifespan. Trends Endocrinol. Metab. 20: 100–106.
- Kayo, T., and A. Koizumi, 1998 Mapping of murine diabetogenic gene mody on chromosome 7 at D7Mit258 and its involvement in pancreatic islet and beta cell development during the perinatal period. J Clin Invest 101: 2112–2118.
- King, E. G., C. M. Merkes, C. L. McNeil, S. R. Hoofer, S. Sen *et al.*, 2012 Genetic dissection of a model complex trait using the

- *Drosophila* synthetic population resource. Genome Res. 22: 1558–1566.
- Lessing, D., and N. M. Bonini, 2008 Polyglutamine genes interact to modulate the severity and progression of neurodegeneration in Drosophila. PLoS Biol. 6: e29.
- Lessing, D., and N. M. Bonini, 2009 Maintaining the brain: insight into human neurodegeneration from Drosophila melanogaster mutants. Nat. Rev. Genet. 10: 359–370.
- Li, L. B., Z. Yu, X. Teng, and N. M. Bonini, 2008 RNA toxicity is a component of ataxin-3 degeneration in Drosophila. Nature 453: 1107–1111.
- Lieschke, G. J., and P. D. Currie, 2007 Animal models of human disease: zebrafish swim into view. Nat. Rev. Genet. 8: 353–367.
- Liu, M., L. Haataja, J. Wright, N. P. Wickramasinghe, Q. X. Hua et al., 2010 Mutant INS-gene induced diabetes of youth: proinsulin cysteine residues impose dominant-negative inhibition on wild-type proinsulin transport. PLoS ONE 5: e13333.
- Ludwig, M. Z., N. A. Tamarina, and R. C. Richmond, 1993 Localization of sequences controlling the spatial, temporal, and sex-specific expression of the esterase 6 locus in Drosophila melanogaster adults. Proc. Natl. Acad. Sci. USA 90: 6233–6237.
- Mackay, T. F., 2010 Mutations and quantitative genetic variation: lessons from Drosophila. Philos. Trans. R. Soc. Lond. B Biol. Sci. 365: 1229–1239.
- Mackay, T. F., 2011 Evolutionary genetics quantified. Nat. Genet. 42: 1033.
- Mackay, T. F., E. A. Stone, and J. F. Ayroles, 2009 The genetics of quantitative traits: challenges and prospects. Nat. Rev. Genet. 10: 565–577.
- Mackay, T. F., S. Richards, E. A. Stone, A. Barbadilla, J. F. Ayroles et al., 2012 The Drosophila melanogaster genetic reference panel. Nature 482: 173–178.
- Mendes, C. S., C. Levet, G. Chatelain, P. Dourlen, A. Fouillet et al., 2009 ER stress protects from retinal degeneration. EMBO J. 28: 1296–1307.
- Mori, K., N. Ogawa, T. Kawahara, H. Yanagi, and T. Yura, 2000 mRNA splicing-mediated C-terminal replacement of transcription factor Hac1p is required for efficient activation of the unfolded protein response. Proc. Natl. Acad. Sci. USA 97: 4660–4665.
- Mozer, B. A., 2001 Dominant Drop mutants are gain-of-function alleles of the muscle segment homeobox gene (msh) whose overexpression leads to the arrest of eye development. Dev. Biol. 233: 380–393.
- Neto-Silva, R. M., B. S. Wells, and L. A. Johnston, 2009 Mechanisms of growth and homeostasis in the Drosophila wing. Annu. Rev. Cell Dev. Biol. 25: 197–220.
- Ocorr, K. A., T. Crawley, G. Gibson, and R. Bodmer, 2007 Genetic variation for cardiac dysfunction in Drosophila. PLoS ONE 2: e601.
- Oyadomari, S., A. Koizumi, K. Takeda, T. Gotoh, S. Akira *et al.*, 2002 Targeted disruption of the Chop gene delays endoplasmic reticulum stress-mediated diabetes. J. Clin. Invest. 109: 525–532
- Palsson, A., and G. Gibson, 2004 Association between nucleotide variation in Egfr and wing shape in *Drosophila melanogaster*. Genetics 167: 1187–1198.
- Pandey, U. B., and C. D. Nichols, 2011 Human disease models in Drosophila melanogaster and the role of the fly in therapeutic drug discovery. Pharmacol. Rev. 63: 411–436.
- Park, S. Y., H. Ye, D. F. Steiner, and G. I. Bell, 2010 Mutant proinsulin proteins associated with neonatal diabetes are retained in the endoplasmic reticulum and not efficiently secreted. Biochem. Biophys. Res. Commun. 391: 1449–1454.
- Park, D., X. Hou, J. V. Sweedler, and P. H. Taghert, 2012 Therapeutic peptide production in Drosophila. Peptides 36: 251–256.

- Passador-Gurgel, G., W. P. Hsieh, P. Hunt, N. Deighton, and G. Gibson, 2007 Quantitative trait transcripts for nicotine resistance in Drosophila melanogaster. Nat. Genet. 39: 264–268.
- Robinow, S., and K. White, 1991 Characterization and spatial distribution of the ELAV protein during Drosophila melanogaster development. J. Neurobiol. 22: 443–461.
- Rudrapatna, V. A., R. L. Cagan, and T. K. Das, 2012 Drosophila cancer models. Dev. Dyn. 241: 107–118.
- Ryoo, H. D., P. M. Domingos, M. J. Kang, and H. Steller, 2007 Unfolded protein response in a Drosophila model for retinal degeneration. EMBO J. 26: 242–252.
- Scheuner, D., and R. J. Kaufman, 2008 The unfolded protein response: a pathway that links insulin demand with beta-cell failure and diabetes. Endocr. Rev. 29: 317–333.
- Schlegel, A., and D. Y. Stainier, 2007 Lessons from "lower" organisms: what worms, flies, and zebrafish can teach us about human energy metabolism. PLoS Genet. 3: e199.
- Shen, X., R. E. Ellis, K. Lee, C. Y. Liu, K. Yang et al., 2001 Complementary signaling pathways regulate the unfolded protein response and are required for C. elegans development. Cell 107: 893–903.
- Song, B., D. Scheuner, D. Ron, S. Pennathur, and R. J. Kaufman, 2008 Chop deletion reduces oxidative stress, improves beta cell function, and promotes cell survival in multiple mouse models of diabetes. J. Clin. Invest. 118: 3378–3389.
- Spradling, A. C., D. M. Stern, I. Kiss, J. Roote, T. Laverty et al., 1995 Gene disruptions using P transposable elements: an integral component of the *Drosophila* genome project. Proc. Natl. Acad. Sci. USA 92: 10824–10830.
- St. Johnston, D., 2002 The art and design of genetic screens: Drosophila melanogaster. Nat. Rev. Genet. 3: 176–188.
- Stoy, J., E. L. Edghill, S. E. Flanagan, H. Ye, V. P. Paz et al., 2007 Insulin gene mutations as a cause of permanent neonatal diabetes. Proc. Natl. Acad. Sci. USA 104: 15040–15044.
- Stoy, J., D. F. Steiner, S. Y. Park, H. Ye, L. H. Philipson et al., 2010 Clinical and molecular genetics of neonatal diabetes due to mutations in the insulin gene. Rev. Endocr. Metab. Disord. 11: 205–215.
- Tabas, I., and D. Ron, 2011 Integrating the mechanisms of apoptosis induced by endoplasmic reticulum stress. Nat. Cell Biol. 13: 184–190.
- Telonis-Scott, M., L. M. McIntyre, and M. L. Wayne, 2005 Genetic architecture of two fitness-related traits in Drosophila melanogaster: ovariole number and thorax length. Genetica 125: 211–222.
- Turner, T. L., and P. M. Miller, 2012 Investigating natural variation in Drosophila courtship song by the evolve and resequence approach. Genetics 191: 633–642.
- Wang, J., T. Takeuchi, S. Tanaka, S. K. Kubo, T. Kayo *et al.*, 1999 A mutation in the insulin 2 gene induces diabetes with severe pancreatic beta-cell dysfunction in the Mody mouse. J. Clin. Invest. 103: 27–37.
- Wang, M. H., L. G. Harshman, and S. V. Nuzhdin, 2005 Quantitative trait loci for lipid content in Drosophila melanogaster. Obes. Res. 13: 1891–1897.
- Wang, Y., D. Pot, S. D. Kachman, S. V. Nuzhdin, and L. G. Harshman, 2006 A quantitative trait locus analysis of natural genetic variation for Drosophila melanogaster oxidative stress survival. J. Hered. 97: 355–366.
- Wang, Y. H., and M. L. Huang, 2009 Reduction of Lobe leads to TORC1 hypoactivation that induces ectopic Jak/STAT signaling to impair Drosophila eye development. Mech. Dev. 126: 781–790.
- Warrick, J. M., H. Y. Chan, G. L. Gray-Board, Y. Chai, H. L. Paulson *et al.*, 1999 Suppression of polyglutamine-mediated neurodegeneration in Drosophila by the molecular chaperone HSP70. Nat. Genet. 23: 425–428.

- Warrick, J. M., L. M. Morabito, J. Bilen, B. Gordesky-Gold, L. Z. Faust *et al.*, 2005 Ataxin-3 suppresses polyglutamine neuro-degeneration in Drosophila by a ubiquitin-associated mechanism. Mol. Cell 18: 37–48.
- Yoshida, H., T. Matsui, A. Yamamoto, T. Okada, and K. Mori, 2001 XBP1 mRNA is induced by ATF6 and spliced by IRE1 in
- response to ER stress to produce a highly active transcription factor. Cell 107:881-891.
- Yu, Z., and N. M. Bonini, 2011 Modeling human trinucleotide repeat diseases in Drosophila. Int. Rev. Neurobiol. 99: 191–212.

Communicating editor: C. Sabatti

GENETICS

Supporting Information

http://www.genetics.org/lookup/suppl/doi:10.1534/genetics.113.157602/-/DC1

Genetic Complexity in a *Drosophila* Model of Diabetes-Associated Misfolded Human Proinsulin

Soo-Young Park, Michael Z. Ludwig, Natalia A. Tamarina, Bin Z. He, Sarah H. Carl, Desiree A. Dickerson, Levi Barse, Bharath Arun, Calvin L. Williams, Cecelia M. Miles, Louis H. Philipson, Donald F. Steiner, Graeme I. Bell, and Martin Kreitman

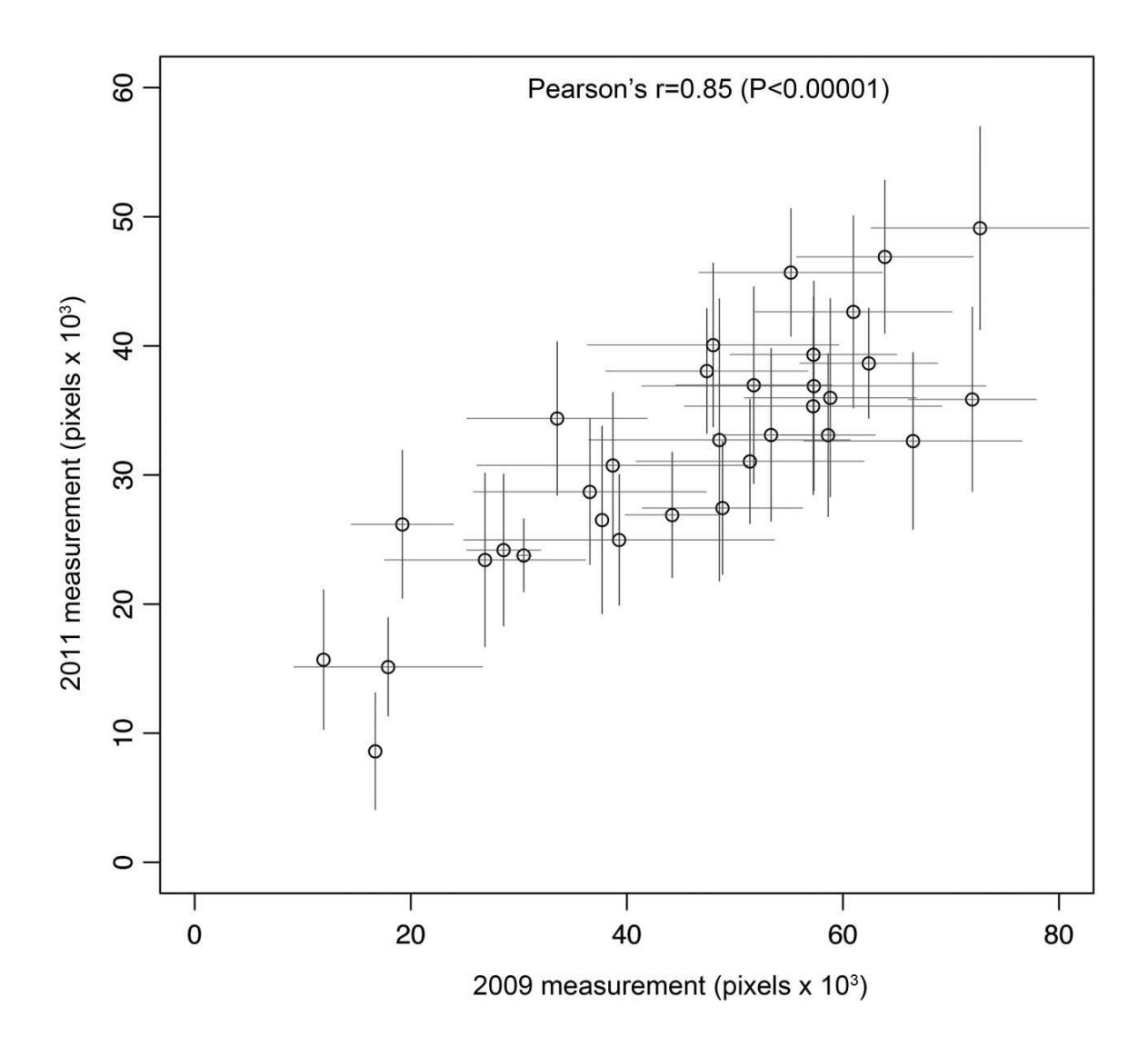


Figure S1 Correlation of GMR>>hINS^{C96Y} eye phenotypes in crosses to DGRP lines. Shown are data collected in two independent experiments carried out in 2009 and 2011. Plotted are average eye areas for approximately 10 males, as described in the Materials & Methods.

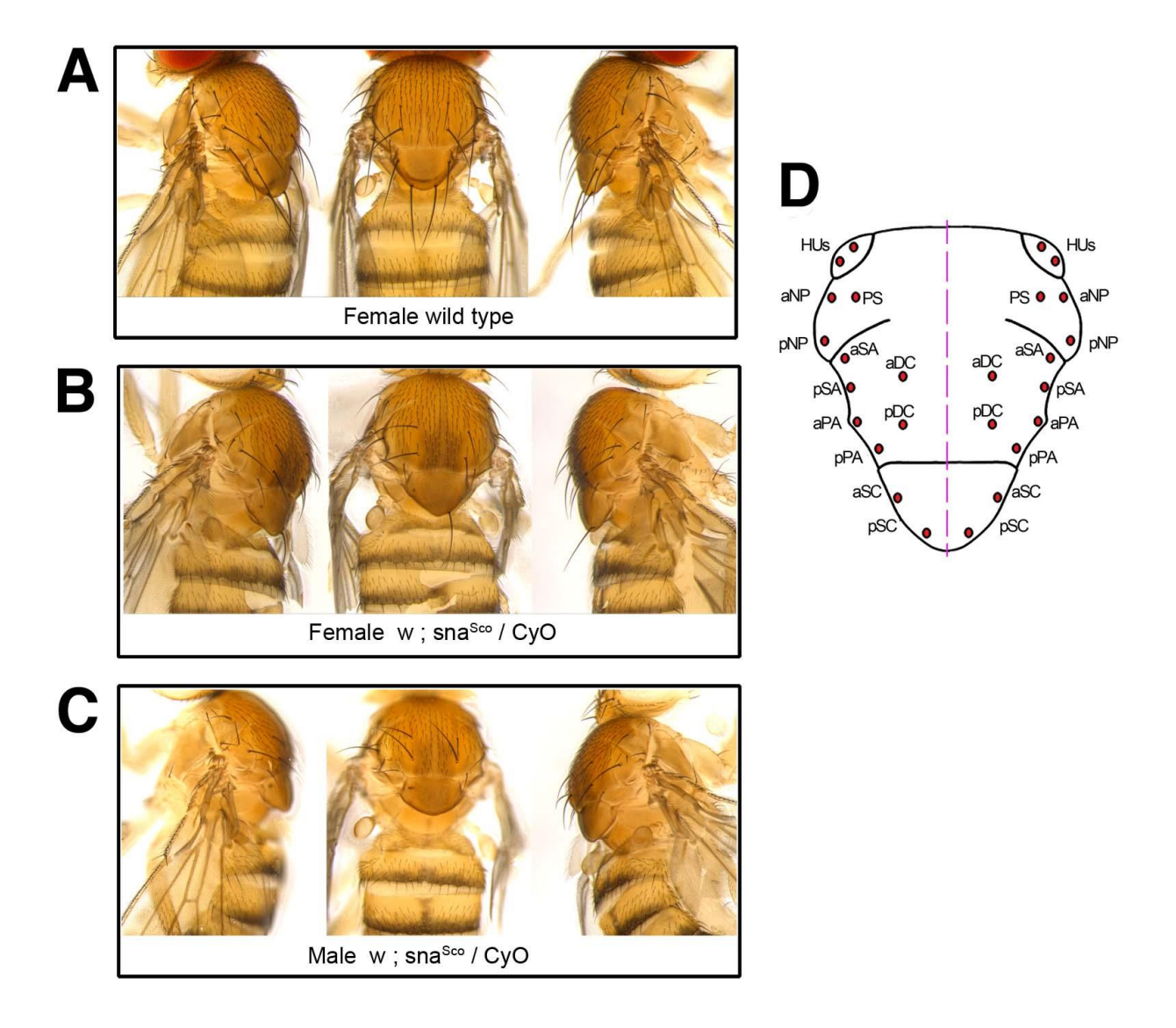
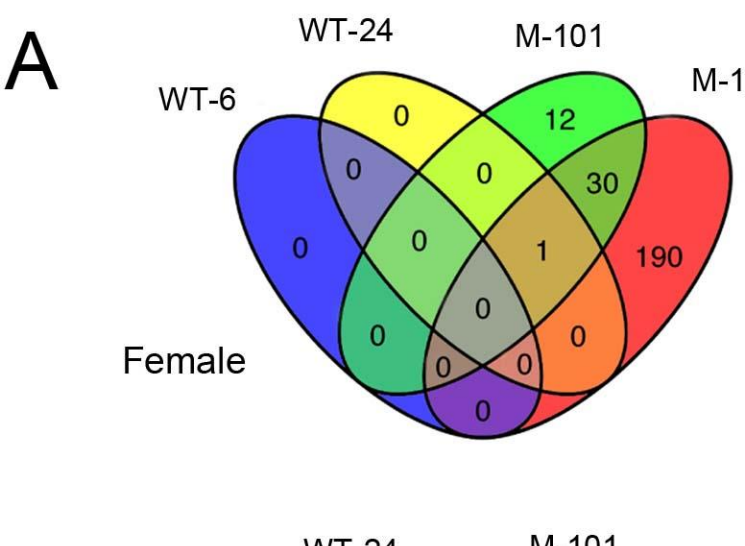


Figure S2 Bristle count. Notum bristles (macrochaete). (A) Wild type female. (B), (C) Notum of Sco mutant (w1118; CyO dfd-YFP / snaSco); (B) female; (C) male. (D) Macrochaete positions on heminotum and humerus with their nomenclature. aDC, anterior dorsocentral bristle; aNP, anterior notopleural bristle; aPA, anterior postalar bristle; aSA, anterior supraalar bristle; aSC, anterior scutellar bristle; HU, humeral bristle. Humeral bristles are prothoracic structures that differentiate from first leg imaginal discs; they were always present in the ap>>hINS^{C96Y} crosses, which is expressed in the mesothorax. Sco mutants, in contrast, often lack humeral bristles, as well as bristles typically lost in ap>>hINS^{C96Y} flies.

S-Y. Park et al. 3 SI



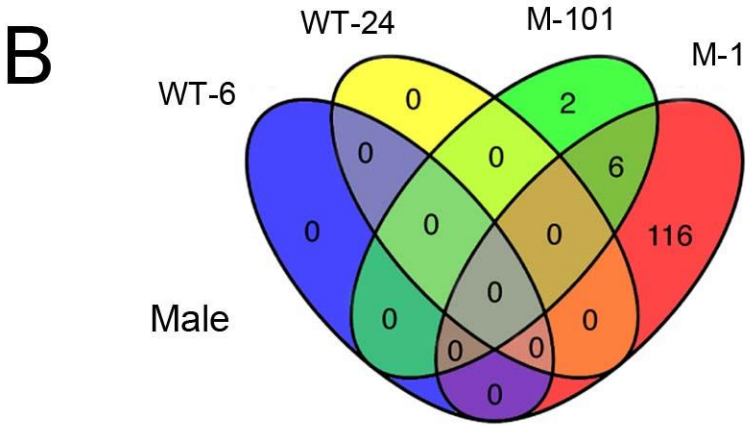
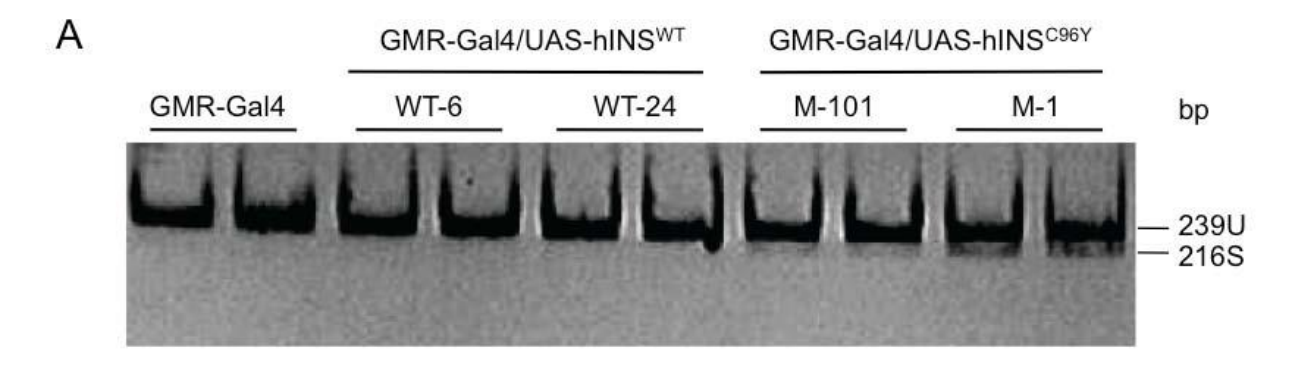


Figure S3 Comparison of gene expression in third-instar eye imaginal discs from GMR-Gal4 and GMR-Gal4 / UAS-hINS^{WT} (Lines WT-6 and WT-24) and GMR-Gal4 / UAS-hINS^{C96Y} (Lines M-101 and M-1). (A) Venn diagram showing differential expression between GMR-Gal4 background and hINS transgenic lines in female larva. (B) Venn diagram showing differential expression between GMR-Gal4 background and hINS transgenic lines in male larva. Expression data were analyzed by sex with one-way ANOVA; significant genes were then tested to determine whether mean expression of hINS^{WT} or hINS^{C96Y} was significantly different from the GMR-Gal4 control (see Data analysis 1 in Material and Methods).



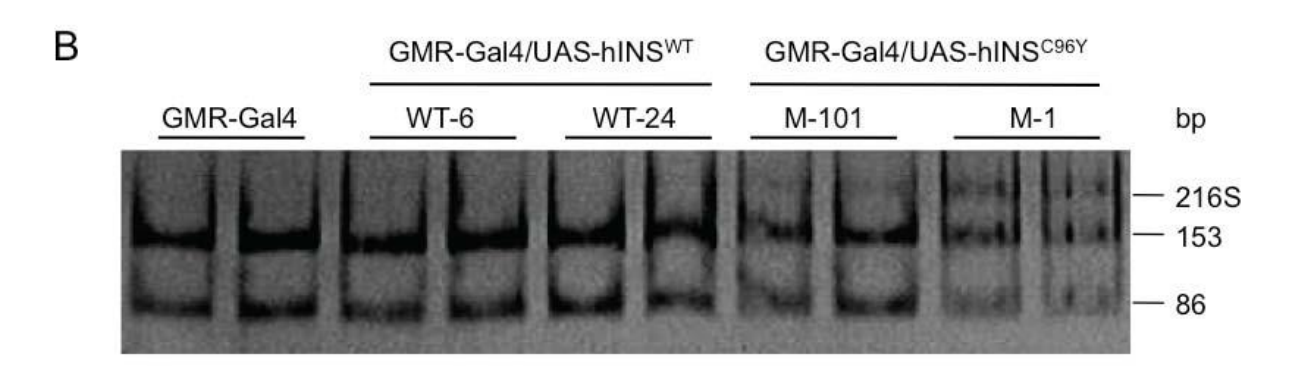


Figure S4 Alternative splicing of XBP1 in RNA. RNA was isolated from eye imaginal discs of 3rd instar larva of indicated genotype. (A) RT-PCR and 10% PAGE analysis of the expression of the XBP1-unspliced (U) and XBP1- spliced (S) transcripts. Unspliced and spliced isoforms could be distinguished by the size of the PCR product (239 and 216 bp, respectively). The PCR products were detected by ethidium bromide staining. (B) To further resolve the two isoforms, the PCR products were treated with *Pst*I to cleave the unspliced form into fragments of 153 and 86 bp.

S-Y. Park et al. 5 SI

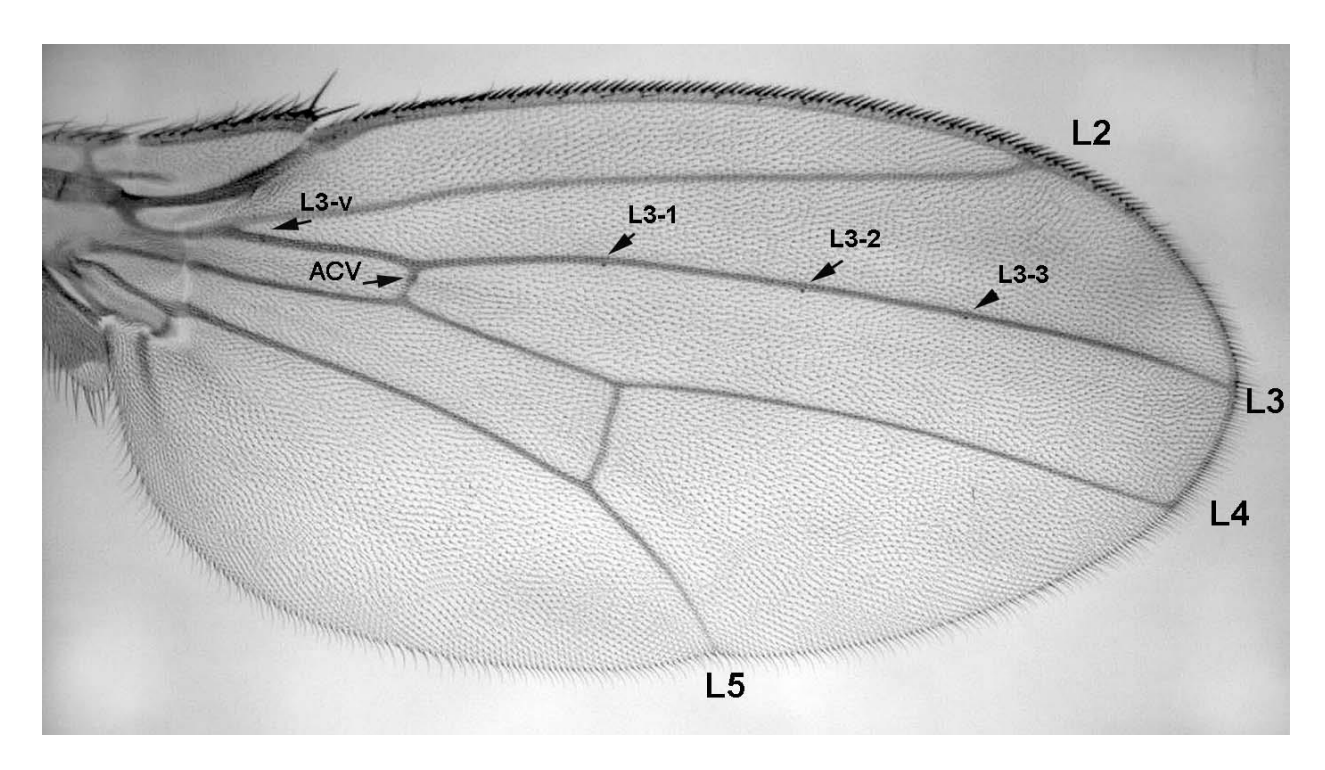


Figure S5 Campaniform sensilla on the wing: L3-v, ACV, L3-1, L3-2, L3-3 (black arrows). L2, L3, L4, and L5: longitudinal veins of the wingblade are numbered.

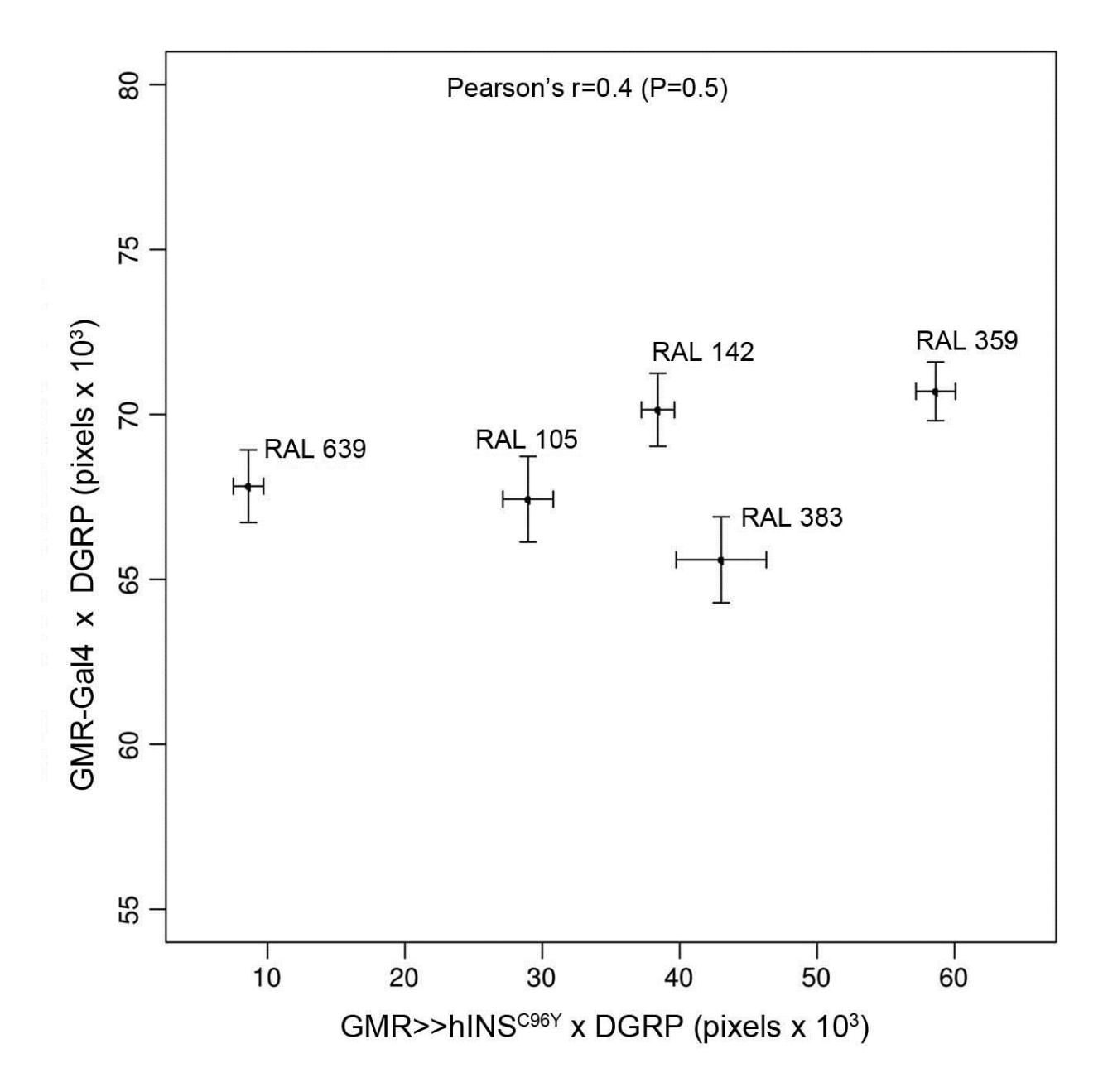


Figure S6 Eye area in crosses of five DGRP lines to hINS^{C96Y} is not correlated with wild type eye area. Five DGRP lines were sampled across the phenotypic distribution of the crosses with hINS^{C96Y}, including the two extremes. They were crossed to a control line (GMR-Gal4), whose male progeny were measured for their eye area. No correlation is observed between results from the hINS^{C96Y} cross and the GMR-Gal4 cross.

S-Y. Park et al. 7 SI

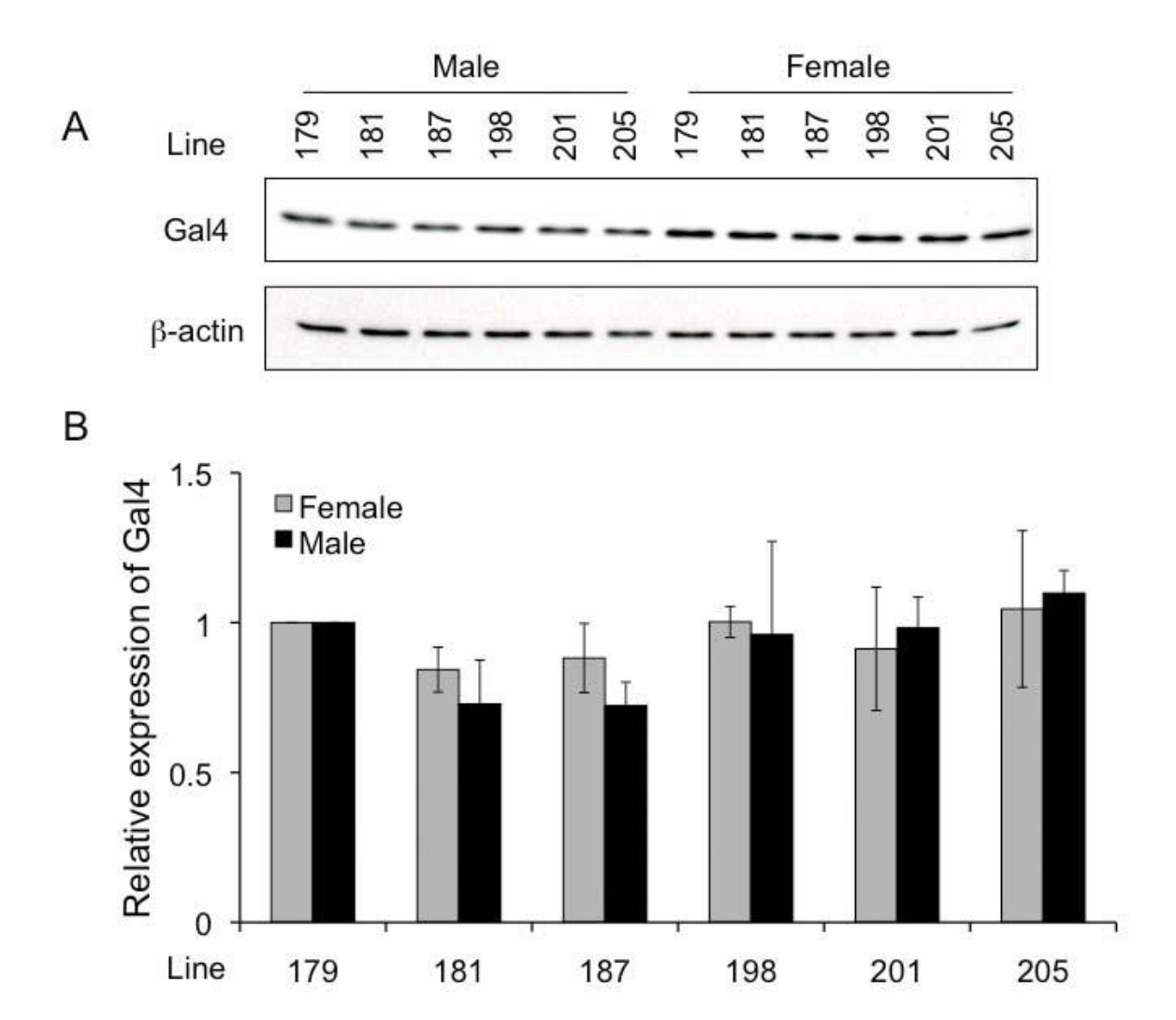


Figure S7 GAL4 concentrations do not differ between DGRP lines in crosses to GMR>>hINS^{C96Y}. (A) Western blot showing Gal4 bands in crosses between GMR>>hINS^{C96Y} and five DGRP lines that were selected to span the range of eye phenotypes, as shown in Figure 5. (B) Mean value of Gal4 expression in two technical replicates. The density of the Gal4 band was normalized to β-actin (control); values shown are the fold change relative to male and female line 179. *Method*: Ten μg of total protein from cell lysates prepared from 20 adult heads was separated on a 10% SDS-PAGE, transferred to a PVDF membrane (Amersham Hybond™-P PVDF Transfer Membrane; GE Healthcare, Piscataway, NJ), and incubated with rabbit polyclonal anti-Gal4 primary antibody (Santa Cruz, CA; sc-577; 1/1,000 dilution and a donkey anti-rabbit IgG-HRP secondary antibody (Santa Cruz, sc-2096; 1/5,000 dilution). The blot was developed with Amersham ECL™ Western Blotting Detection Reagents and detected by chemiluminescence. The blot was also probed with a mouse β-actin antibody (Santa Cruz; sc-47778; 1/1,000 dilution) as a loading control. Band intensity was quantified using the Gel Analysis package in ImageJ Software (NIH).

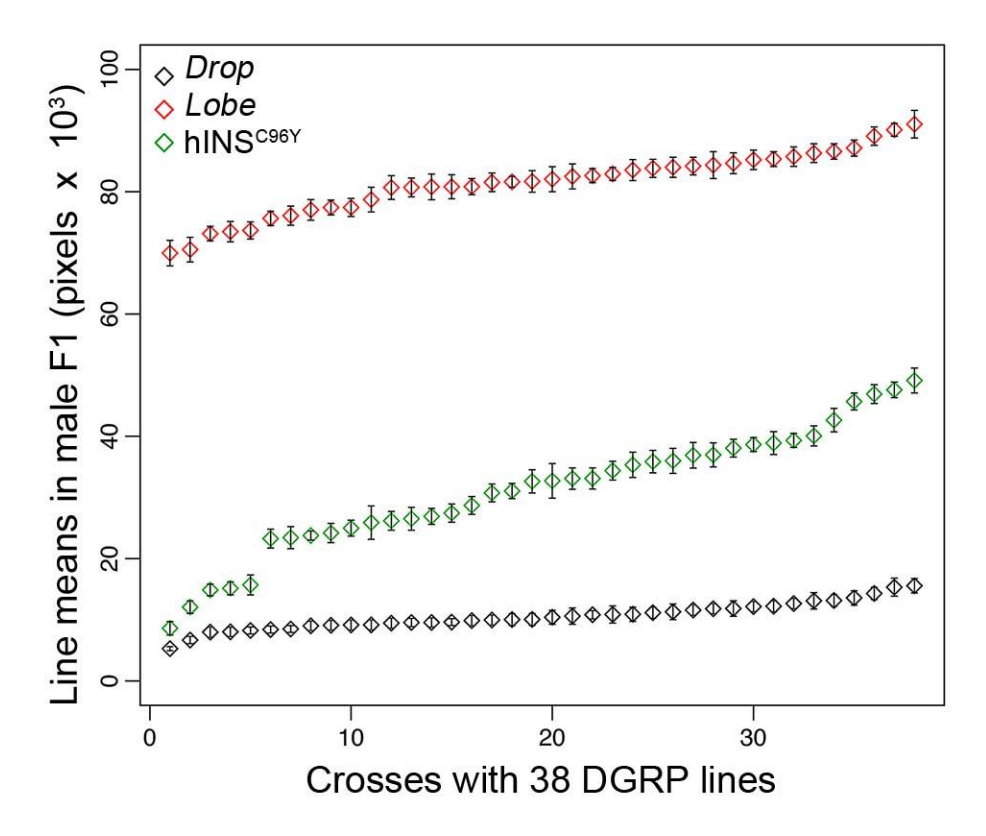


Figure S8 Untransformed eye areas in F_1 adults produced from crosses of Dr, L, or GMR>>hINS^{C96Y} to DGRP lines. Data shown are mean \pm SE. Although Dr and L eye area varies less than GMR>>hINS^{C96Y}, the between-line (i.e., heritable) differences are comparable when scaled by within-line variances (Figure 7).

Files S1-S2

Available for download as Excel files at http://www.genetics.org/lookup/suppl/doi:10.1534/genetics.113.157602/-/DC1

File S1 189 genes up-regulated by GMR-Gal4/UAS-hINS^{C96Y} in male eye imaginal disc, 108 genes down-regulated by GMR-Gal4/UAS-hINS^{C96Y} in male eye imaginal disc, 81 genes up-regulated by GMR-Gal4/UAS-hINS^{C96Y} in female eye imaginal disc, and 28 genes down-regulated by GMR-Gal4/UAS-hINS^{C96Y} in female eye imaginal disc

File S2 Top 514 genes based on Anova

Table S1 Primer sequences used for quantitative real-time PCR

Gene	Forward	Reverse
Human proinsulin	CTACCTAGTGTGCGGGGAAC	GCTGGTAGAGGGAGCAGATG
CG4583 (IRE1)	GAGATCACAGCGAACGACAA	GGATAATTCGGCTGTCCTCA
CG2087 (PEK)	GTGGTTCTGGTGGAAGGAAA	GGCACATGACGTTCAATGAC
CG4147 (Hsc70-3)	CAAGTTCGAGGAGCTCAACC	AATCTCGTGCACGTCCTTCT
CG9415 (XBP1)	AGAACCACAAGCTGGACTCG	CAGATCCAAGGTTGGTGGAC
CG3966	TGGCTGCCAGTTTTATGTGA	CGGGTAGAACTCGAACTGCT
CG7130	ACAAGATTCTGGGCATCGAG	CGCGCTTTTCCTTATCAAAG
CG10420	GGAGGCAAGACAAGCTGAAG	TAGCTTGACCTTCCGCAATC
CG10160	TTTAGAGGCGCCCAAAATAA	GAGACGTTCTGAGCCAGGAT
CG9150	CGAAGGTCACGTTCTCATCA	TAACCCGGATTTTGTTCGAG

Table S2 Selected genes up-regulated by GMR-Gal4/UAS-hINS^{C96Y} in male eye imaginal discs

Probe set	Transcript	Name	Description (GO) ¹	Homolog ²
Transport				
1634512_at ³	CG5226-RA	CG5226	Carnitine transport	SLC6A17
1637439_at	CG14709-RA	Mrp4	Transport	ABCC4
1635700_at ³	CG31792-RA	CG31792-RA	Ion transport	
1627582_a_at	CG30035-RA	Tret1	Trehalose transport	SLC2A8
1624450_at	CG6331-RA	Orct	Ion transport	
1623247_at ³	CG10420-RA	CG10420	Intracellular protein	SIL1
			membrane transport	
1636800_at ³	CG13610-RA	Orct2	Ion transport	
1641606_s_at ³	CG6608-RB	Tpc1	Thiamine pyrophosphate	
			transport	
1632622_	CG32538-RB	GfA	Ion transport	
1629040_at	CG3476-RA	CG3476	Ion transport	
1633039_at ³	CG5646-RA	CG5646	Mitochondrial transport	
			(acyl carnitine)	
1627945_at³	CG4205-RA	Fdxh	Electron transport	FDX1L
1625250_at	CG5802-RA	CG5802	Sugar transport	SLC35B1
1630804_at*	CG6417-RA	Oatp33Eb	lon transport	
1633536_at	CG4630-RA	CG4630	Transport	
1635684_a_at	CG2999-RA	unc-13	Synaptic vesicle exocytosis	UNC13C
1641511_at	CG7394-RA	TIM14	Membrane transport	DNAJC19
1623743_at	CG3191-RA	CG3191	Transport	
1631763_at	CG31793-RA	CG31793	Transport	ABCC4
1637280_at	CG4861-RA	LpR1	Receptor-mediated	VLDLR
			endocytosis	
1640075_a_at	CG3424-RA	pathetic	Transport	
1640220_a_at	CG11779-RA	CG11779	Transport	TIMM44
1633304_at	CG1967-RA	p24-1	Post-Golgi vesicle-mediated transport	TMED7

1632676_s_at ³	CG11897-RA	CG11897	Transport	
1637772_at	CG4726-RA	MFS3	Ion transport	
1631856_a_at	CG7361-RB	RFeSP	Transport	UQCRFS1
Oxidation-reduction	<u>1</u>			
1635227_at ³	CG10160-RA	ImpL3	Oxidoreductase	LDHA
1639033_at ³	CG9432-RB	I(2)01289	Oxidoreductase	
1638053_at ³	CG10842-RA	Cyp4p1	Oxidoreductase	
1637063_at	CG33099-RA	CG33099	Oxidoreductase	
1623971_at ³	CG9150-RA	CG9150	Oxidoreductase	
1623787_at	CG7144-RA	CG7144	Oxidoreductase	AASS
1627525_a_at	CG1333-RA	Ero1L	Oxidoreductase	ERO1LB
1630885_at ³	CG12534-RA	Alr	Oxidoreductase	GFER
1627945_at ³	CG4205-RA	Fdxh	Oxidoreductase	FDX1L
1638006_at	CG10211-RA	CG10211	Oxidoreductase	
1633687_at	CG13611-RA	CG13611	Oxidoreductase	
1636759_at	CG8303-RA	CG8303	Oxidoreductase	
1624571_s_at ³	CG32857-RA	CG32857	Oxidoreductase	
1624003_at	CG10639-RA	CG10639	Oxidoreductase	
1634019_at	CG2064-RA	CG2064	Oxidoreductase	RDH12
1640566_at	CG1944-RA	Cyp4p2	Oxidoreductase	
1632676_s_at ³	CG11897-RA	CG11897	Oxidoreductase	
1631856_a_at	CG7361-RB	RFeSP	Oxidoreductase	UQCRFS1
1633238_at	CG17533-RA	GstEB	Oxidoreductase	
1630258_at	CG4181-RA	GstD2	Oxidoreductase	
Mitochondrial prote	<u>ein</u>			
1634658_a_at	CG8772-RD	Nemy	Mitochondrion	GLS
1641606_s_at ³	CG6608-RB	Tpc1	Mitochondrion	
1629040_at	CG3476-RA	CG3476	Mitochondrion	
1633039_at ³	CG5646-RA	CG5646	Mitochondrion	
1630885_at ³	CG12534-RA	Air	Mitochondrion	GFER

S-Y. Park *et al.* 13 SI

1639676_at ³	CG15173-RA	Ttc19	Mitochondrion	
1627945_at ³	CG4205-RA	Fdxh	Mitochondrion	FDX1L
1641511_at	CG7394-RA	TIM14	Mitochondrion	DNAJC19
1626460_at	CG2658-RA	CG2658	Mitochondrion	
1627034_a_a	CG9410-RB	Coq10	Mitochondrion	
1640220_a_at	CG11779-RA	CG11779	Mitochondrion	TIMM44
1627939_a_at ³	CG2098-RA	Fech	Mitochondrion	FECH
1625763_at	CG2789-RA	CG2789	Mitochondrion	TSPO
1640566_at	CG1944-RA	Cyp4p2	Mitochondrion	
1631856_a_at	CG7361-RB	RFeSP	Mitochondrion	UQCRFS1
1634899_a_at	CG6512-RA	CG6512	Mitochondrion	AFG3L2

¹ GO molecular function/process from <u>www.flybase.org</u>, <u>www.uniprot.org</u> and <u>www.david.abcc.ncifcrf.gov</u>

 $^{^2}$ Human homolog from <u>www.flight.icr.ac.uk</u>

³ Up-regulated in female and male

Table S3 Selected genes down-regulated by GMR-Gal4/UAS-hINS^{C96Y} in male eye imaginal discs

Probe set	Transcript	Name	Description (GO) ¹	Homolog ²
Regulation of transc	cription			
1624663_a_at ³	CG8821-RA	Vismay	DNA binding	
1635500_a_at	CG17228-RA	Prospero	DNA binding	
1631408_at	CG18024-RA	SoxNeuro	DNA binding	SOX1
1633592_a_at	CG5413-RB	CREG	Transcription repressor	CREG1
1630105_at	CG3891-RA	Nuclear factor Y-box A	DNA binding	NFYA
1636931_at	CG11491-RD	Broad	DNA binding	QRFPR
1626045_at ³	CG31318-RA	Rpb4	Transcription factor	TADA2L
1639732_s_at ⁴	CG4881-RA	Spalt-related	RNA polymerase II	SALL1
			Transcription factor	
Ion Binding				
1638311_at	CG12817-RA	CG12817	Ion binding	
1633488_at ⁴	CG3705-RA	astray	Ion binding	PSPH
1630163_at ³	CG32373-RA	CG32373	Ion binding	
1629347_at	CG12296-RA	klu	Ion binding	
1633000_a_at	CG7100-RA	CadN	Ion binding	SQRDL
1641652_a_at	CG33166-RB	stet	Ion binding	RHBDL3
1630504_at	CG13830-RA	CG13830	Ion binding	
1636602_at	CG11253-RA	CG11253	Ion binding	
1624001_at	H DC07119	Scribbler	Ion binding	
1624617_at	CG1665-RA	CG1665	Ion binding	
1630434_a_at	CG31064-RA	CG31064	Ion binding	RUFY2
1639969_at	CG6969-RA	Cardinal	Ion binding	
1635447_at	CG4827-RA	veil	Ion binding	NT5E
1636931_at	CG11491-RD	Broad	Ion binding	QRFPR
1626045_at ³	CG31318-RA	Rpb4	Ion binding	TADA2L
1635580_at	CG7037-RB	Cbl	Ion binding	CBL
1624039_at	CG10147-RA	CG10147	Ion binding	

S-Y. Park *et al.* 15 SI

1638682_a_at	CG11988-RC	Neur	Ion binding	NEURL1B
1640696_at	CG17803-RA	CG17803	Ion binding	
Enzyme activity				
1633488_at ⁴	CG3705-RA	Astray	Phosphatase	PSPH
1624505_at	CG6113-RA	Lip4	Lipase	LIPA
1634351_at ⁴	CG7860-RA	CG7860	Asparaginase	
1627360_at	CG31349-RF	Polychaetoid	Guanylate kinase	TJP1
1626045_at ³	CG31318-RA	Rpb4	Acetyltransferase	TADA2L
1623299_at ³	CG1794-RA	Mmp2	Endopeptidase	MMP2
1628149_a_at³	CG14895-RB	Pak3	Protein kinase	PAK3

¹ GO molecular function/process from <u>www.flybase.org</u>, www.uniprot.org and <u>www.david.abcc.ncifcrf.gov</u>

 $^{^2}$ Human homolog from $\underline{www.flight.icr.ac.uk}$

³ Down-regulated in female and male

⁴ Down-regulated only in female

Table S4 Functional annotation clustering

Cluster_1 Enrichment_Score; 2.4 SP_PIR_KEYWORDS Membrane 40 3.10E-04 GOTERM_CC_FAT Integral to membrane 40 0.004 GOTERM_CC_FAT Intrinsic to membrane 40 0.006 SP_PIR_KEYWORDS Transmembrane 33 0.006 UP_SEQ_FEATURE Transmembrane region 19 0.026 Cluster_2 Enrichment_Score: 1.38 GOTERM_CC_FAT Cell projection 7 0.021 GOTERM_CC_FAT Neuron projection 4 0.054 GOTERM_CC_FAT Dendrite 3 0.063 Cluster_3 Enrichment_Score: 1.32 Cluster_A Cluster_Barries 6 0.004 GOTERM_MF_FAT Iron-sulfur cluster binding 6 0.004 Cluster_SPIR_KEYWORDS 2Fe-2S 3 0.022 GOTERM_MF_FAT 2 iron, 2 sulfur cluster binding 3 0.046 SP_PIR_KEYWORDS Iron-sulfur 3 0.089 SP_PIR_KEYWORDS Iron-sulfur 3 0.089 SP_PIR_KEYWORDS Transit pept	Database	Keywords	Count	P-value
GOTERM_CC_FAT Integral to membrane 40 0.004 GOTERM_CC_FAT Intrinsic to membrane 40 0.006 SP_PIR_KEYWORDS Transmembrane 33 0.006 UP_SEQ_FEATURE Transmembrane region 19 0.026 Cluster_2 Enrichment_Score: 1.38	Cluster_1	Enrichment_Score: 2.4		
GOTERM_CC_FAT Intrinsic to membrane 40 0.006 SP_PIR_KEYWORDS Transmembrane 33 0.006 UP_SEQ_FEATURE Transmembrane region 19 0.026 Cluster_2 Enrichment_Score: 1.38	SP_PIR_KEYWORDS	Membrane	40	3.10E-04
SP_PIR_KEYWORDS Transmembrane 33 0.006 UP_SEQ_FEATURE Transmembrane region 19 0.026 Cluster_2 Enrichment_Score: 1.38	GOTERM_CC_FAT	Integral to membrane	40	0.004
Cluster_2 Enrichment_Score: 1.38 GOTERM_CC_FAT Cell projection 7 0.021 GOTERM_CC_FAT Neuron projection 4 0.054 GOTERM_CC_FAT Dendrite 3 0.063 Cluster_3 Enrichment_Score: 1.32 Semantial contents Concept of the contents	GOTERM_CC_FAT	Intrinsic to membrane	40	0.006
Cluster_2 Enrichment_Score: 1.38 GOTERM_CC_FAT Cell projection 7 0.021 GOTERM_CC_FAT Neuron projection 4 0.054 GOTERM_CC_FAT Dendrite 3 0.063 Cluster_3 Enrichment_Score: 1.32	SP_PIR_KEYWORDS	Transmembrane	33	0.006
GOTERM_CC_FAT Cell projection 7 0.021 GOTERM_CC_FAT Neuron projection 4 0.054 GOTERM_CC_FAT Dendrite 3 0.063 Cluster_3 Enrichment_Score: 1.32 GOTERM_MF_FAT Iron-sulfur cluster binding 6 0.004 GOTERM_MF_FAT Metal cluster binding 6 0.004 SP_PIR_KEYWORDS 2Fe-2S 3 0.022 GOTERM_MF_FAT 2 iron, 2 sulfur cluster binding 3 0.046 SP_PIR_KEYWORDS Iron-sulfur 3 0.089 SP_PIR_KEYWORDS Mitochondrion 7 0.150 SP_PIR_KEYWORDS Transit peptide 4 0.380 UP_SEQ_FEATURE Transit peptide:Mitochondrion 4 0.400	UP_SEQ_FEATURE	Transmembrane region	19	0.026
GOTERM_CC_FAT Cell projection 7 0.021 GOTERM_CC_FAT Neuron projection 4 0.054 GOTERM_CC_FAT Dendrite 3 0.063 Cluster_3 Enrichment_Score: 1.32 GOTERM_MF_FAT Iron-sulfur cluster binding 6 0.004 GOTERM_MF_FAT Metal cluster binding 6 0.004 SP_PIR_KEYWORDS 2Fe-2S 3 0.022 GOTERM_MF_FAT 2 iron, 2 sulfur cluster binding 3 0.046 SP_PIR_KEYWORDS Iron-sulfur 3 0.089 SP_PIR_KEYWORDS Mitochondrion 7 0.150 SP_PIR_KEYWORDS Transit peptide 4 0.380 UP_SEQ_FEATURE Transit peptide:Mitochondrion 4 0.400				
GOTERM_CC_FAT Neuron projection 4 0.054 GOTERM_CC_FAT Dendrite 3 0.063 Cluster_3 Enrichment_Score: 1.32 GOTERM_MF_FAT Iron-sulfur cluster binding 6 0.004 GOTERM_MF_FAT Metal cluster binding 6 0.004 SP_PIR_KEYWORDS 2Fe-2S 3 0.022 GOTERM_MF_FAT 2 iron, 2 sulfur cluster binding 3 0.046 SP_PIR_KEYWORDS Iron-sulfur 3 0.089 SP_PIR_KEYWORDS Mitochondrion 7 0.150 SP_PIR_KEYWORDS Transit peptide 4 0.380 UP_SEQ_FEATURE Transit peptide:Mitochondrion 4 0.400	Cluster_2	Enrichment_Score: 1.38		
Cluster_3 Enrichment_Score: 1.32 GOTERM_MF_FAT Iron-sulfur cluster binding 6 0.004 GOTERM_MF_FAT Metal cluster binding 6 0.004 SP_PIR_KEYWORDS 2Fe-2S 3 0.022 GOTERM_MF_FAT 2 iron, 2 sulfur cluster binding 3 0.046 SP_PIR_KEYWORDS Iron-sulfur 3 0.089 SP_PIR_KEYWORDS Mitochondrion 7 0.150 SP_PIR_KEYWORDS Transit peptide UP_SEQ_FEATURE Transit peptide:Mitochondrion 4 0.400	GOTERM_CC_FAT	Cell projection	7	0.021
Cluster_3 Enrichment_Score: 1.32 GOTERM_MF_FAT Iron-sulfur cluster binding 6 0.004 GOTERM_MF_FAT Metal cluster binding 6 0.004 SP_PIR_KEYWORDS 2Fe-2S 3 0.022 GOTERM_MF_FAT 2 iron, 2 sulfur cluster binding 3 0.046 SP_PIR_KEYWORDS Iron-sulfur 3 0.089 SP_PIR_KEYWORDS Mitochondrion 7 0.150 SP_PIR_KEYWORDS Transit peptide 4 0.380 UP_SEQ_FEATURE Transit peptide:Mitochondrion 4 0.400	GOTERM_CC_FAT	Neuron projection	4	0.054
GOTERM_MF_FAT Iron-sulfur cluster binding 6 0.004 GOTERM_MF_FAT Metal cluster binding 6 0.004 SP_PIR_KEYWORDS 2Fe-2S 3 0.022 GOTERM_MF_FAT 2 iron, 2 sulfur cluster binding 3 0.046 SP_PIR_KEYWORDS Iron-sulfur 3 0.089 SP_PIR_KEYWORDS Mitochondrion 7 0.150 SP_PIR_KEYWORDS Transit peptide 4 0.380 UP_SEQ_FEATURE Transit peptide:Mitochondrion 4 0.400	GOTERM_CC_FAT	Dendrite	3	0.063
GOTERM_MF_FAT Iron-sulfur cluster binding 6 0.004 GOTERM_MF_FAT Metal cluster binding 6 0.004 SP_PIR_KEYWORDS 2Fe-2S 3 0.022 GOTERM_MF_FAT 2 iron, 2 sulfur cluster binding 3 0.046 SP_PIR_KEYWORDS Iron-sulfur 3 0.089 SP_PIR_KEYWORDS Mitochondrion 7 0.150 SP_PIR_KEYWORDS Transit peptide 4 0.380 UP_SEQ_FEATURE Transit peptide:Mitochondrion 4 0.400				
GOTERM_MF_FAT Metal cluster binding 6 0.004 SP_PIR_KEYWORDS 2Fe-2S 3 0.022 GOTERM_MF_FAT 2 iron, 2 sulfur cluster binding 3 0.046 SP_PIR_KEYWORDS Iron-sulfur 3 0.089 SP_PIR_KEYWORDS Mitochondrion 7 0.150 SP_PIR_KEYWORDS Transit peptide 4 0.380 UP_SEQ_FEATURE Transit peptide:Mitochondrion 4 0.400	Cluster_3	Enrichment_Score: 1.32		
SP_PIR_KEYWORDS2Fe-2S30.022GOTERM_MF_FAT2 iron, 2 sulfur cluster binding30.046SP_PIR_KEYWORDSIron-sulfur30.089SP_PIR_KEYWORDSMitochondrion70.150SP_PIR_KEYWORDSTransit peptide40.380UP_SEQ_FEATURETransit peptide:Mitochondrion40.400	GOTERM_MF_FAT	Iron-sulfur cluster binding	6	0.004
GOTERM_MF_FAT 2 iron, 2 sulfur cluster binding 3 0.046 SP_PIR_KEYWORDS Iron-sulfur 3 0.089 SP_PIR_KEYWORDS Mitochondrion 7 0.150 SP_PIR_KEYWORDS Transit peptide 4 0.380 UP_SEQ_FEATURE Transit peptide:Mitochondrion 4 0.400	GOTERM_MF_FAT	Metal cluster binding	6	0.004
SP_PIR_KEYWORDSIron-sulfur30.089SP_PIR_KEYWORDSMitochondrion70.150SP_PIR_KEYWORDSTransit peptide40.380UP_SEQ_FEATURETransit peptide:Mitochondrion40.400	SP_PIR_KEYWORDS	2Fe-2S	3	0.022
SP_PIR_KEYWORDS Mitochondrion 7 0.150 SP_PIR_KEYWORDS Transit peptide 4 0.380 UP_SEQ_FEATURE Transit peptide:Mitochondrion 4 0.400	GOTERM_MF_FAT	2 iron, 2 sulfur cluster binding	3	0.046
SP_PIR_KEYWORDS Transit peptide 4 0.380 UP_SEQ_FEATURE Transit peptide:Mitochondrion 4 0.400	SP_PIR_KEYWORDS	Iron-sulfur	3	0.089
UP_SEQ_FEATURE Transit peptide:Mitochondrion 4 0.400	SP_PIR_KEYWORDS	Mitochondrion	7	0.150
	SP_PIR_KEYWORDS	Transit peptide	4	0.380
Cluster_4 Enrichment_Score: 1.12	UP_SEQ_FEATURE	Transit peptide:Mitochondrion	4	0.400
Cluster_4 Enrichment_Score: 1.12				
	Cluster_4	Enrichment_Score: 1.12		
SMART DnaJ 4 0.054	SMART	DnaJ	4	0.054
INTERPRO Heat shock protein DnaJ, N-terminal 4 0.059	INTERPRO	Heat shock protein DnaJ, N-terminal	4	0.059
GOTERM_MF_FAT Heat shock protein binding 4 0.061	GOTERM_MF_FAT	Heat shock protein binding	4	0.061
INTERPRO Molecular chaperone, heat shock protein, 3 0.180	INTERPRO	Molecular chaperone, heat shock protein,	3	0.180
Hsp40, DnaJ		Hsp40, DnaJ		

S-Y. Park et al. 17 SI

In total 385 probe sets identified as differentially expressed in either sexes were used in this analysis. 30 of the 385 probe_sets were removed in the most recent Affymetrix annotation, leaving 355. Functional annotation clustering were done using the DAVID web service (ref), with the default choice of annotation terms (excluding GOTERM_BP_FAT) and medium clustering criteria. Changing either the terms or the clustering criteria won't affect the general result. For example, the heat shock protein cluster is always among the top clusters in various settings.

Table S5 Quantitative real-time PCR

Gene	GMR-Gal4	GMR-Gal4/UAS-hINSWT		GMR-Gal4/UAS-	hINS ^{C96Y}
		WT-6	WT-24	M-101	M-1
IRE1	1.05 ± 0.23	$\textbf{1.12} \pm \textbf{0.12}$	$\textbf{1.37} \pm \textbf{0.28}$	1.99 ± 0.22	1.78 ± 0.23
				(P=0.04)	(P=0.08)
PEK ¹	$\boldsymbol{1.00 \pm 0.04}$	0.89 ± 0.11	$\textbf{1.11} \pm \textbf{0.13}$	1.99 ± 0.15	1.98 ± 0.15
				(P=0.003)	(P=0.0007)
Hsc70-3 ²	$\textbf{1.11} \pm \textbf{0.36}$	0.91 ± 0.27	0.74 ± 0.07	1.50 ± 0.06	$\textbf{2.75} \pm \textbf{0.22}$
			(P=0.38)		(P=0.0176)
XBP1	$\textbf{1.05} \pm \textbf{0.25}$	$\textbf{1.50} \pm \textbf{0.24}$	$\textbf{1.55} \pm \textbf{0.23}$	2.03 ± 0.17	$\textbf{2.22} \pm \textbf{0.25}$
				(P=0.03)	(P=0.03)

Comparison of gene expression of upstream regulators of UPR in male 3^{rd} instar larval eye imaginal discs is shown. The results was normalized to the expression level of rp49 and compared to GMR-Gal4 using an unpaired t-test. The data are shown as mean \pm SE and the exact P-values are shown.

S-Y. Park *et al.* 19 SI

¹ Human homolog of PKR-like ER kinase (PERK)

² Human homolog of BiP (also known as GRP78)

Table S6 Comparison of gene expression levels by microarray and quantitative real-time PCR

A. Microarray

Gene	GMR-Gal4	GMR-Gal4/UAS-hINSWT		GMR-Gal4/L	JAS-hINS ^{C96Y}
		WT-6	WT-24	M-101	M-1
CG3966	1.00 ± 0.23	0.89 ± 0.00	0.87 ± 0.12	1.32 ± 0.09	6.27 ± 1.08*
CG7130	$\textbf{1.00} \pm \textbf{0.02}$	0.96 ± 0.02	$\textbf{1.12} \pm \textbf{0.14}$	$1.78 \pm 0.04*$	3.90 ± 0.36 *
CG10420	$\boldsymbol{1.00\pm0.09}$	$\textbf{1.03} \pm \textbf{0.05}$	0.96 ± 0.07	$1.98 \pm 0.07*$	$2.55 \pm 0.37*$
CG10160	$\boldsymbol{1.00\pm0.13}$	1.36 ± 0.15	1.03 ±0.15	12.63 ± 0.16 *	15.45 ± 1.76*
CG9150	1.00 ± 0.02	$\textbf{1.03} \pm \textbf{0.02}$	0.85 ± 0.15	1.80 ± 0.06 *	2.70 ± 0.56*

B. Quantitative RT-PCR

Gene	GMR-Gal4	GMR-Gal4/	GMR-Gal4/UAS-hINSWT		AS-hINS ^{C96Y}
		WT-6	WT-24	M-101	M-1
CG3966	1.01 ± 0.08	0.98 ± 0.08	1.16 ± 0.05	$1.97 \pm 0.14*$	9.1 ± 0.93*
CG7130	1.00 ± 0.02	$\textbf{0.84} \pm \textbf{0.21}$	0.99 ± 0.03	$\textbf{1.66} \pm \textbf{0.13*}$	4.03 ± 0.71 *
CG10420	1.01 ± 0.08	$\textbf{1.12} \pm \textbf{0.06}$	$\textbf{1.03} \pm \textbf{0.14}$	$4.81 \pm 0.43*$	$11.77 \pm 0.44*$
CG10160	1.01 ± 0.09	1.11 ± 0.35	$\boldsymbol{0.70 \pm 0.22}$	234.64 ± 80.76*	378 ± 64.08*
CG9150	$\textbf{1.02} \pm \textbf{0.12}$	1.18 ± 0.32	1.02 ± 0.08	$2.49 \pm 0.07*$	$3.73 \pm 0.38*$

Gene expression was normalized to the expression level of rp49 and compared to GMR-Gal4 using an unpaired t-test. Data are shown as mean \pm SE.

^{*} P < 0.05

Table S7 Number of Missing Bristles

	ap>>hINS ^{C96Y} / CyO	ap>>hINS ^{C96Y} X W1118	Sco X w1118	
Female	6.56 ± 1.80	8.32 ± 2.14	9.20 ±1.44	
Male	10.92 ± 2.33	13.36 ± 2.48	9.36 ±1.32	

We recombined the ap-GAL4 driver onto the chromosome containing the M-1 UAS-hINS^{C96Y} transgene to create ap>>hINS^{C96Y}. Sco (Scutoid) also reduces bristles on the notum to approximately the same level as mutant hINS. We used Sco in a control cross to investigate whether it has a sex-biased bristle phenotype. The fact that it does not suggests that the sex-biased phenotype produced by mutant hINS may not be through sex-specific inputs to bristle formation but rather through a physiological difference in the response of male and female somatic cells to mutant hINS protein. Data are shown as mean ± SD.

Table S8 Missing or displaced companiform sensilla

Sex	en>>hINS ^{WT}	en>>hINS ^{C96Y}	dpp>>hINS ^{WT}	dpp>>hINS ^{C96Y}
Female	0	7	0	11
Male	0	4	1	14

We examined four sensilla — one on the ACV and three along L3 (see Figure S5) — from one wing in 10 individuals. Tabulated are the total number of displaced sensillae out of 40.

Table S9 Correlation between mutations and sexes

	Drop	Lobe	GMR>>hINS ^{C96Y}	ap>>hINS ^{C96Y}
Drop	0.63*	0.2	0.06	-0.19
Lobe	0.09	0.53*	0.08	-0.12
GMR>>hINS ^{C96Y}	0.13	-0.07	0.88*	-0.23
ap>>hINS ^{C96Y}	-0.19	0.29	-0.17	0.67*

Diagonal elements are correlations between the two sexes for each mutation group; the upper triangle contains correlations between males in the respective mutation groups, and numbers in the lower triangle area are for females. Pearson's correlation is calculated for all pairs except those involving the bristle number, in which case the Spearman's correlation (rank correlation) is calculated. * indicates a correlation test P < 0.05 (P-values corrected for multiple testing using Bonferroni method)

S-Y. Park et al. 23 SI

Table S10 Effect of genetic variation on eye area and bristle number in females

		Drop	Lobe	ap>>INS ^{C96Y}
DGRP Line	Eye area	Eye area	Eye area	Number of Bristles
RAL-208	64.58 ± 6.99	$\textbf{14.60} \pm \textbf{4.01}$	94.66 ± 5.69	$\textbf{23.1} \pm \textbf{2.0}$
RAL-301	66.59 ± 5.81	16.88 ± 3.88	97.50 ± 4.73	25.2 ± 1.0
RAL-303	61.25 ± 6.32	14.01 ± 1.88	94.54 ± 4.86	24.5 ± 1.5
RAL-304	66.87 ± 27.85	14.63 ± 2.43	97.36 ± 5.79	23.8 ± 1.9
RAL-307	$\textbf{80.10} \pm \textbf{8.11}$	15.08 ± 4.20	101.84 ± 6.73	25.7 ± 0.5
RAL-313	68.62 ± 5.47	14.22 ± 4.33	91.99 ± 8.85	25.8 ± 0.5
RAL-315	47.58 ± 4.55	9.61 ± 1.82	82.04 ± 4.74	23.9 ± 2.2
RAL-324	67.72 ± 4.65	$\textbf{11.02} \pm \textbf{1.92}$	NA	24.9 ± 0.9
RAL-335	63.11 ± 6.28	$\textbf{12.38} \pm \textbf{1.82}$	96.48 ± 7.63	18.6 ± 2.1
RAL-357	68.49 ± 11.45	13.53 ± 2.19	86.01 ± 9.87	25.6 ± 0.6
RAL-358	$\textbf{70.18} \pm \textbf{4.91}$	16.39 ± 3.63	$\textbf{95.36} \pm \textbf{6.01}$	25.2 ± 1.3
RAL-360	69.02 ± 6.85	13.30 ± 2.60	95.21 ± 13.73	23.9 ± 1.4
RAL-362	37.29 ± 4.37	24.21 ± 8.91	98.77 ± 7.44	24.8 ± 1.0
RAL-375	55.85 ± 6.87	14.05 ± 1.83	91.55 ± 5.53	24.0 ± 1.3
RAL-379	59.42 ± 6.15	$\textbf{16.02} \pm \textbf{3.10}$	98.02 ± 5.42	24.4 ± 1.2
RAL-380	69.96 ± 4.07	11.89 ± 1.83	93.38 ± 5.33	20.5 ± 2.1
RAL-391	48.63 ± 6.85	$\textbf{15.43} \pm \textbf{4.56}$	87.50 ± 8.92	23.8 ± 2.2
RAL-399	43.31 ± 8.51	13.75 ± 2.93	97.43 ± 8.47	25.2 ± 0.9
RAL-427	53.88 ± 12.51	19.65 ± 6.10	96.57 ± 9.69	25.8 ± 0.5
RAL-437	$\textbf{70.21} \pm \textbf{8.30}$	16.73 ± 3.03	101.10 ± 5.44	23.5 ± 1.4
RAL-486	60.40 ± 5.79	17.66 ± 3.51	$\textbf{96.22} \pm \textbf{6.41}$	23.4 ± 1.3
RAL-426	63.41 ± 8.99	12.88 ± 1.58	95.91 ± 7.65	23.3 ± 1.5
RAL-517	71.37 ± 5.08	10.40 ± 1.87	104.17 ± 6.48	24.6 ± 1.2
RAL-555	56.32 ± 8.91	$\textbf{13.77} \pm \textbf{3.18}$	101.21 ± 5.35	23.0 ± 1.9
RAL-639	28.56 ± 15.68	13.60 ± 2.78	95.42 ± 5.39	23.2 ± 2.1
RAL-707	$\textbf{71.94} \pm \textbf{6.69}$	$\textbf{14.27} \pm \textbf{2.12}$	103.78 ± 6.82	25.2 ± 0.9

RAL-712	59.56 ± 6.67	13.57 ± 3.86	73.41 ± 22.28	25.7 ± 0.7
RAL-730	61.14 ± 10.99	14.54 ± 2.89	101.73 ± 5.57	25.3 ± 1.0
RAL-732	55.86 ± 7.85	12.50 ± 1.80	96.72 ± 8.16	23.9 ± 1.5
RAL-765	50.59 ± 11.68	13.56 ± 1.74	62.45 ± 20.45	24.0 ± 0.8
RAL-774	67.71 ± 7.20	13.68 ± 2.19	$\textbf{91.80} \pm \textbf{7.02}$	25.8 ± 0.4
RAL-786	54.59 ± 7.48	$\textbf{12.54} \pm \textbf{1.76}$	94.26 ± 6.55	25.6 ± 0.6
RAL-799	59.45 ± 5.81	13.21 ± 3.85	99.35 ± 7.31	24.0 ± 1.2
RAL-820	55.22 ± 10.40	14.10 ± 2.23	101.15 ± 5.98	25.1 ± 1.0
RAL-852	$\textbf{72.05} \pm \textbf{6.21}$	14.60 ± 3.26	81.69 ± 16.53	24.8 ± 0.9
RAL-365	76.59 ± 4.88	14.03 ± 3.49	99.59 ± 7.13	25.4 ± 0.9
RAL-705	52.63 ± 7.89	13.68 ± 2.14	95.56 ± 7.65	24.4 ± 1.1
RAL-714	68.74 ± 6.30	12.54 ± 3.62	NA	25.0 ± 1.2

The eye area or dorsal bristle number were measured in 10 individuals. The eye area (pixels \times 10³) and number of bristles are shown as mean \pm SE.

S-Y. Park et al. 25 SI

Table S11 Effect of genetic variation on eye area and bristle number in males

	GMR>>INS ^{C96Y}	Drop	Lobe	ap>>INS ^{C96Y}
DGRP Line	Eye area	Eye area	Eye area	Number of Bristles
RAL-208	25.55 ± 4.76	9.15 ± 2.71	80.79 ± 7.57	19.8 ± 1.5
RAL-301	32.33 ± 5.56	11.16 ± 3.14	73.46 ± 6.20	18.3 ± 3.9
RAL-303	$\textbf{31.41} \pm \textbf{6.53}$	9.87 ± 2.99	$\textbf{73.67} \pm \textbf{5.44}$	$\textbf{23.3} \pm \textbf{1.6}$
RAL-304	39.92 ± 7.34	10.87 ± 4.85	76.08 ± 6.08	$\textbf{21.0} \pm \textbf{2.0}$
RAL-307	46.12 ± 7.40	15.56 ± 4.26	$\textbf{91.04} \pm \textbf{7.14}$	$\textbf{23.4} \pm \textbf{1.5}$
RAL-313	36.76 ± 6.94	$\textbf{8.25} \pm \textbf{1.89}$	86.30 ± 5.75	24.7 ± 1.4
RAL-315	22.38 ± 2.72	6.68 ± 2.12	$\textbf{73.13} \pm \textbf{4.60}$	19.8 ± 1.8
RAL-324	44.29 ± 4.23	$\textbf{7.98} \pm \textbf{2.92}$	75.63 ± 4.38	$\textbf{23.4} \pm \textbf{1.1}$
RAL-335	35.77 ± 4.32	8.02 ± 2.39	77.02 ± 5.83	$\textbf{11.0} \pm \textbf{1.1}$
RAL-357	36.14 ± 4.49	11.80 ± 3.11	$\textbf{81.68} \pm \textbf{6.35}$	25.1 ± 1.2
RAL-358	34.04 ± 6.96	11.84 ± 4.18	82.04 ± 7.65	$\textbf{22.4} \pm \textbf{2.0}$
RAL-360	30.18 ± 10.04	12.16 ± 3.32	85.21 ± 6.17	$\textbf{22.4} \pm \textbf{1.8}$
RAL-362	70.52 ± 7.21	13.10 ± 5.01	82.63 ± 4.26	24.0 ± 1.1
RAL-375	29.00 ± 5.43	$\textbf{12.65} \pm \textbf{2.79}$	83.53 ± 6.19	$\textbf{20.1} \pm \textbf{2.5}$
RAL-379	$\textbf{27.05} \pm \textbf{5.47}$	12.22 ± 3.35	85.32 ± 4.69	21.6 ± 2.2
RAL-380	36.80 ± 6.07	9.01 ± 2.70	80.68 ± 6.72	$\textbf{13.7} \pm \textbf{2.2}$
RAL-391	13.83 ± 3.61	13.57 ± 4.38	70.53 ± 6.69	$\textbf{21.9} \pm \textbf{1.9}$
RAL-399	10.65 ± 3.48	10.03 ± 3.37	$\textbf{81.53} \pm \textbf{5.45}$	$\textbf{17.9} \pm \textbf{2.5}$
RAL-427	25.96 ± 5.16	14.30 ± 3.63	87.13 ± 4.94	25.6 ± 0.7
RAL-437	33.82 ± 7.29	13.15 ± 3.60	85.73 ± 5.73	20.7 ± 2.3
RAL-486	30.94 ± 6.10	11.30 ± 4.44	89.08 ± 5.77	22.4 ± 1.8
RAL-426	30.93 ± 6.49	9.16 ± 2.82	80.82 ± 5.12	20.6 ± 2.0
RAL-517	29.32 ± 4.64	$\textbf{5.27} \pm \textbf{1.09}$	90.12 ± 3.94	21.5 ± 1.9
RAL-555	23.27 ± 4.74	9.55 ± 2.63	83.83 ± 5.54	$\textbf{21.9} \pm \textbf{1.9}$
RAL-639	$\textbf{7.13} \pm \textbf{4.47}$	8.40 ± 2.25	84.64 ± 6.59	21.1 ± 2.2
RAL-707	34.95 ± 7.72	9.97 ± 3.12	78.70 ± 7.26	23.4 ± 1.4

RAL-712	31.96 ± 7.29	9.55 ± 2.42	80.80 ± 6.80	23.8 ± 1.4
RAL-730	23.92 ± 9.50	$\textbf{15.32} \pm \textbf{7.03}$	77.42 ± 5.74	22.6 ± 1.5
RAL-732	21.65 ± 5.90	$\textbf{10.90} \pm \textbf{4.01}$	84.35 ± 6.96	19.6 ± 2.5
RAL-765	13.46 ± 5.90	9.62 ± 2.12	80.69 ± 5.55	19.7 ± 1.6
RAL-774	24.75 ± 5.48	8.49 ± 1.94	69.95 ± 6.60	25.5 ± 0.7
RAL-786	22.51 ± 5.73	11.58 ± 3.17	83.99 ± 6.38	24.7 ± 1.5
RAL-799	24.51 ± 7.25	9.10 ± 2.72	81.61 ± 3.29	21.0 ± 2.1
RAL-820	21.97 ± 6.59	10.59 ± 4.59	82.90 ± 4.00	24.3 ± 1.7
RAL-852	34.65 ± 7.39	10.82 ± 2.65	86.58 ± 4.90	14.1 ± 2.8
RAL-365	43.91 ± 5.69	9.45 ± 2.96	77.41 ± 4.70	23.9 ± 1.4
RAL-705	13.90 ± 3.58	10.40 ± 4.10	82.48 ± 7.07	18.8 ± 2.4
RAL-714	42.56 ± 5.22	10.05 ± 3.41	84.19 ± 4.99	24.0 ± 1.9

The eye area or dorsal bristle number were measured in 10 individuals. The eye area (pixels \times 10³) and number of bristles are shown as mean \pm SE.

S-Y. Park et al. 27 SI